Electrochemical and Photoelectrochemical Properties of the Copper Hydroxyphosphate Mineral Libethenite

by

Man Li

A Thesis Presented in Partial Fulfillment
of the Requirements for the Degree
Master of Science

Approved June 2013 by the
Graduate Supervisory Committee:

Candace Chan, Chair
Michael O'Connell
Peter Crozier

ARIZONA STATE UNIVERSITY

August 2013

ABSTRACT

There has been much interest in photoelectrochemical conversion of solar energy in recent years due to its potential for low-cost, sustainable and renewable production of fuels. Despite the huge potential, there are still a number of technical barriers due to the many constraints needed in order to drive photoelectrochemical reactions such as overall water splitting and the identification of efficient and effective semiconductor materials. To this end, the search for novel semiconductors that can act as light absorbers is still needed. The copper hydroxyphosphate mineral libethenite (CHP), which has a chemical formula of $Cu_2(OH)PO_4$, has been recently shown to be active for photocatalytic degradation of methylene blue under UV-irradiation[1,2], indicating that photo-excited electrons and holes can effectively be generated and separated in this material. However, CHP has not been well studied and many of its fundamental electrochemical and photoelectrochemical properties are still unknown. In this work, the synthesis of different morphologies of CHP using hydrothermal synthesis and precipitation methods were explored. Additionally, a preliminary investigation of the relevant fundamental characteristics such as the bandgap, flatband potential, band diagram, electrochemical and photoelectrochemical properties for CHP was performed. Better understanding of the properties of this material may lead to the development of improved catalysts and photocatalysts from natural sources.

ACKNOWLEGEMENTS

This thesis was finished under my advisor Dr. Candace Chan's kind concern and concentrated guidance. I would like to thank her for her instruction and help. She has devoted a large amount of energy to it. It has been an enjoyable experience to work with her.

I would like to thank Emmanuel Soignard and David Wright for their help with X-ray diffraction and Karl Weiss and Sisouk Phrasavath for their assistance with the electron microscopes. I would like to thank all my friends here at Arizona State University for their friendship and the moments we spent together, especially Qian Cheng, Ting Yang, and Ran Zhao, who gave me a hand with my research.

We gratefully acknowledge the use of facilities within the LeRoy Eyring Center for Solid State Science at Arizona State University.

Most importantly, I would like to thank my parents for their love and support.

TABLE OF CONTENTS

LIST OF FIGURES

1. Introduction

Solar energy can be explained as the radiant light and heat that comes from the sun. Humans have begun to utilize it since ancient times using a range of different technologies. Solar energy technologies, which also can be called solar energy conversion technologies, include solar heating, solar photovoltaics, solar thermal electricity, fuels generated using solar energy (i.e. solar fuels), and photoelectrochemical cells. These technologies allow solar energy conversion to make a considerable contribution to solving the energy problems that the world faces nowadays, such as the shortage of the fuel energy[3,4].

The International Energy Agency said in 2011 that "the development of affordable, inexhaustible and clean solar energy technologies will have huge longer-term benefits. It will increase countries' energy security through reliance on an indigenous, inexhaustible and mostly import-independent resource, enhance sustainability, reduce pollution, lower the costs of mitigating climate change, and keep fossil fuel prices lower than otherwise. These advantages are global. Hence the additional costs of the incentives for early deployment should be considered learning investments; they must be wisely spent and need to be widely shared"[3].

One of the many research fields which show promise for solar energy conversion is photoelectrochemistry[5]. In recent years, there has been much interest in photoelectrochemical conversion of solar energy particularly in the application of photoelectrochemical systems to the problem of solar energy

conversion and storage[6], due to the potential for low-cost, sustainable and renewable production of fuels and electricity. Photoelectrochemical processes usually use solar energy to drive electrochemical reactions while involving transformation of light energy, including visible light, to produce fuels such as hydrogen from water[7]. These processes can offset the shortage of fuel energy and also can convert solar energy into storable and transportable fuels. To be more specific, these processes usually involve semiconducting materials as electrodes in a liquid cell to generate electrons and holes upon illumination, which result in electrochemical reactions at the surface of both electrodes.

The first time that the photoeffects at electrodes in electrochemical cells were observed was by Becquerel in 1839 [8], when the photoelectrochemical experiment was first performed. The origin of this photovoltaic phenomenon is called the "Becquerel effect", which demonstrated that the potential of certain electrodes changed when illuminated. However, this effect was not fully understood until Brattain and Garrett [9] launched the modern epoch of photoelectrochemistry in 1954.

Generally speaking, the photoelectrochemical cell (PEC) is a cell or device where a semiconducting material as one electrode is illuminated in a liquid cell and drives electrochemical reactions at both electrodes. Some PECs simply produce electrical energy while others can generate hydrogen or oxygen in a process similar to the electrolysis of water. This is called photoelectrochemical water splitting, which is to dissociate water using either artificial or natural light

into its constituent parts, hydrogen (H_2) and oxygen (O_2). Nowadays, photocatalytic water splitting using semiconductor materials attracts considerable attention since it decomposes water, an inexpensive renewable resource, to provide a clean and renewable fuel such as H_2 utilizing abundant solar light, which has no adverse effects on the atmosphere.

1.1. Photocatalyst

According to the definition of PEC, materials that can be used as photo-electrodes must meet two basic requirements----the optical function and catalytic function, which means they are required to absorb solar energy and to drive reactions such as water splitting. As a result, semiconductor photocatalysts can play the role here since they satisfy those requirements.

However, the search for effective semiconductor photocatalysts is challenging due to the many constraints needed in order to drive photoelectrochemical reactions such as overall water splitting and the identification of efficient and effective semiconductor materials. One of the biggest challenges is that many semiconductors are not stable to photocorrosion in water. To this end, the search for novel semiconductors that can act as light absorbers is still needed. Given that oxides are the most stable materials to photocorrosion, there has been a great deal of investigation into the photoelectrochemical performance of oxide materials. To date, research on photoanodes for water oxidation has focused predominately on metal oxides such as TiO_2, WO_3, and Fe_2O_3.

In 1969, the photodecomposition of water at a TiO_2 electrode was first demonstrated by Fujishima et al.[10], which initiated a new era for photocatalysts. During that time, photocatalysis with TiO_2 including some other semiconducting titanates such as $SrTiO_3$ and $BaTiO_3$ [11] . TiO_2 photocatalysts have been successfully applied to a number of industrial processes, like hydrogen and oxygen production, effluents detoxification and disinfection, and organic synthesis[12-16]. Until now, TiO_2 is primarily used in PECs as a photocatalyst to achieve substantial efficiency.

However, TiO_2 is not ideal for all purposes because the material absorbs only UV radiation. To this end, there has been a lot of investigation to further improve the performance, such as the modification of its microstructure like in porous nanocrystalline TiO_2 photoelectrochemical cells[17], energy band modulation by doping with elements such as N, C, and S[18,19],and the construction of hetero-junctions by combining TiO_2 with metals such as Pt or Pd[20-22]. Simultaneously, inspired by TiO_2, the use of conventional semiconductors such WO_3 in photocatalysis has been investigated by Reiche et al.[23] in the search for possible alternatives to TiO_2.

In recent years, significant progress has been made in the development of novel nanomaterials, especially since nanocrystalline iron oxide (α-Fe_2O_3) has been shown to have more efficiency for photocatalyzing water oxidation[24]. Iron oxide is an n-type semiconductor with a band gap of 2.1 eV, which is smaller than the bandgap for TiO_2, which allows for the absorption of a significant portion of

the visible sun light. Through the construction of nanostructured α-Fe_2O_3 electrodes that can effectively decrease charge carrier recombination[25-31], poor charge transport problems in α-Fe_2O_3 have been alleviated to some extent. Nanomaterials can provide large surface areas, abundant surface states, diverse morphologies and shorter carrier diffusion length, all of which are properties beneficial to photocatalysis.

Despite the huge potential, however, even with several decades of research, there have been few advances in the identification of oxides with significantly better solar energy conversion properties. The efficiency of photocatalytic nanomaterials must be improved to meet engineering requirements, and the stability and cost of these materials should also be carefully considered. Thus, it is important to expand our scope of investigation beyond the traditional oxide materials.

1.2. Phosphate-containing Materials

It is important to develop simple and low cost semiconductor photocatalytic materials composed of inexpensive and abundant elements that are also stable both chemically and photochemically[32-34].

Phosphate-containing materials in general are known for their mechanical, chemical and thermal stabilities. Phosphorus is the 10th most abundant element on Earth and phosphate minerals have a rich and diverse crystal chemistry[35]. Hence, phosphate materials may be promising candidates for the investigation of new photocatalyst or electrocatalyst materials. Recently, there has been a great deal of

interest in phosphate-containing systems since the discovery of the amorphous cobalt-phosphate (Co-Pi) catalyst in 2008 by Matthew W. Kanan et al.[36], which displays high activity for water oxidation at a neutral solution in the range of pH 7-9. To prepare the catalyst, they applied a controlled potential to Co^{2+} salts in pH 7 phosphate (Pi) buffer at 1.3 V (vs. NHE). The current asymptotically approached 1.5 mA/cm^2 over several hours and a dark green-black film was observed to form on the surface of the electrode surface during this time. Similar behavior was observed by Surendranath et al. when methyl phosphonate (MePi) was used as the supporting electrolyte instead of phosphate[37]. Later in 2010, Diane et. al.[38] came up with an idea to electrodeposit cobalt−phosphate water oxidation catalyst ("Co−Pi") onto mesostructured α-Fe_2O_3 photoanodes. The photoelectrochemical properties of the resulting composite photoanodes was optimized for solar water oxidation in neutral electrolytes pH 8. The Co-Pi oxygen evolution catalyst advances the viability of solar driven water-splitting by enabling the solar-to-fuels conversion to be performed in neutral water as a solar storage mechanism.

Furthermore, researchers Zhiguo Yi et. al. have also shown that a simple semiconductor material, Ag_3PO_4, can serve as a photocatalyst for water oxidation and degradation of organic contaminants[39]. They reported that the Ag_3PO_4 material can efficiently oxidize water but is also reduced simultaneously under visible-light irradiation (λ < 530 nm).

Even though those discoveries attract a great deal of interest in phosphate-containing materials serving as water oxidation catalysts for researchers, the development of phosphate-containing materials as photocatalysts or electrocatalysts still need to be further explored. The worthy thing is that those investigations can indicate a direction for later research on expanding the scope of developing simple and low cost semiconductor photocatalytic materials.

1.3. Copper Hydroxyphosphate

Considering the entire class of phosphate materials, a naturally occurring copper hydroxyphosphate $Cu_2(OH)PO_4$, also known as the mineral libethenite, from here on abbreviated as CHP, has come to the attention of researchers. CHP presents itself as a particularly interesting starting point for exploring the electrochemical properties of phosphates for use as electrocatalysts and photocatalysts.

The structure of CHP consists of $Cu_2O_6(OH)_2$ dimers and 1-dimensional $Cu_2O_6(OH)_2$ chains linked by PO_4 tetrahedra (Fig. 1). The bridging hydroxyl group is a unique feature of the CHP structure and is thought to be the source of highly active hydroxyl radicals that impart catalytic activity.

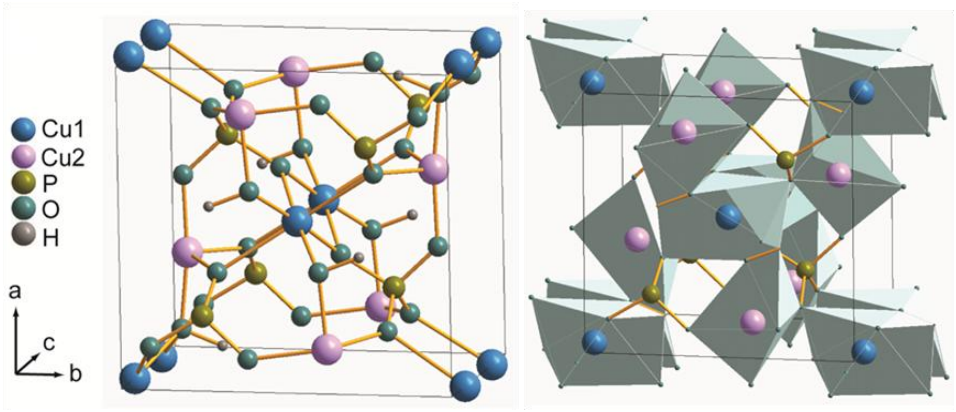

(a) (b)

Figure 1. (a) Ball and stick and (b) polyhedron configuration of the libethenite unit cell

CHP has been recently shown to have catalytic activity for oxidation of olefins and alcohols, hydroxylation of phenol, and epoxidation of styrene[40,41] by forming highly active hydroxyl radicals[42]. It has also recently been shown to be active for photocatalytic degradation of organic dyes under UV-irradiation[1,2,43], even demonstrating higher activity than WO_3 and P25 TiO_2. It has also been suggested to have activity for decomposition of 2,4-dichlorophenol under near-infrared absorption[44]. These studies indicate that photo-excited electrons and holes can be effectively generated and separated in this material. However, CHP has not been well studied and many of the fundamental materials and photoelectrochemical properties are still unknown.

To this end, I have conducted a preliminary investigation of the relevant fundamental characteristics such as the bandgap, flatband potential, electrochemical and photoelectrochemical properties for CHP. Better

understanding of this material may lead to the development of improved catalysts and photocatalysts from natural sources.

To be more specific, in my M.S. thesis work, I have first investigated the preparation of libethenite (CHP) materials by different synthesis methods such as precipitation and hydrothermal approaches, followed by structural and morphological evaluation by powder x-ray diffraction (XRD) and scanning electronic microscope (SEM). The CHP electrodes were fabricated by coating a viscous slurry or a thin paste of the CHP powder onto fluorine-doped tin oxide (FTO) glass or Au coated FTO using doctor blading or electrophoretic deposition (EPD). Measurements were performed to investigate the relevant fundamental characteristics such as the bandgap, flatband potential, and band diagram of CHP. Further discussion of the electrochemical and photoelectrochemical properties of CHP was achieved by decorating RuO_2, a highly active electrocatalyst for water oxidation, on the CHP electrode, and adding hole scavengers such as methanol and hydrogen peroxide in the electrolyte.

Key objectives for my project are to understand the photoelectrochemical and electrochemical properties of copper hydroxyphosphates. Potential outcomes of the project are: (1) creation of fundamental knowledge regarding the properties of new hydroxyphosphate based materials, (2) development of an earth abundant catalyst based on natural minerals for reactions such as water oxidation.

1.4. Characterization Techniques

1.4.1. X-ray Diffraction

The X-ray diffraction (XRD) technique is one of the most useful methods to identify phases and for determining the atomic and molecular structure in materials such as metals, ceramics, minerals, polymers, or other inorganic and organic compounds. The atomic planes of a crystal can cause the incident beam of X-rays to interfere with one another as they leave the crystal and diffract into many specific directions. The scattered X-rays are collected by the detector and produce a diffraction pattern made of reflections from the atomic planes in the material. By measuring the angles and intensities of these diffracted beams, the signals of the reflections are shown as peaks in the XRD pattern and can be used to identify the crystal structure of the material.

1.4.2. Scanning Electron Microscopy

The scanning electron microscope (SEM) uses a focused beam of high-energy electrons, instead of using light to form an image, to generate a variety of signals at the surface of samples. The signals that are derived from electron-sample interactions can reveal information about the sample including external morphology, chemical composition and so on. Since its development in the early 1950's, scanning electron microscopy has become one of the most commonly used techniques for examining a sample’s morphology in research today and developed new areas of study in the physical, chemical and many other science communities. The scanning electron microscope has many advantages over

traditional microscopes because the wavelength of electrons is much smaller than that of visible light. Closely spaced specimens can be magnified at much higher levels and the degree of magnification can be controlled much more by the researcher because of its much higher resolution.

Generally speaking, in a SEM machine, a high tension electron beam is focused onto the sample and scans across it. As the incident electron beam interacts with electrons in the sample, secondary electrons are generated producing various signals that can be detected. These detected signals are collected to form an image of the sample that contains information about the sample's surface topography and composition.

Because SEM utilizes vacuum conditions and uses electrons to form the image, the appropriate special preparation must be performed. Water must be removed completely from the samples because vapor from the water would affect the vacuum condition. Non-metallic materials need to be made conductive by adhering them to a conducting tape or by covering the sample with a thin layer of conductive material such as gold using a sputter coater.

1.4.3. Photoelectrochemical Measurement

Photoelectrochemical measurements are usually conducted in a photoelectrochemical cell (PEC) and controlled with a potentiostat. In a typical photoelectrochemical cell, there are three electrodes connected to the potentiostat: the working electrode (WE), reference electrode (RE), and counter electrode (CE) which is usually Pt wire.

1.4.3.1. Linear Sweep Voltammetry

Linear sweep voltammetry (LSV) is a voltammetric technique where the current between a working electrode and counter electrode is measured as the potential between the working electrode and a reference electrode is swept at a certain scan rate. Cyclic voltammetry (CV) is a form of LSV where a backward scan is done in the opposite potential direction as well. Oxidation or reduction of species is indicated through a peak or rise in the current signal at the potential where the species begins to be oxidized or reduced. Additionally, by comparing the current curve under dark condition and illumination conditions, the photocurrent can be acquired.

1.4.3.2. Chronoamperometry

Chronoamperometry (CA) is an electrochemical technique involving stepping the potential of the working electrode from an initial potential, generally at which no Faradaic reaction occurs, to a potential E_i, at which the Faradaic reaction occurs. The basis of the controlled-potential technique is to measure the current response to an applied potential step. The current vs. time curve reflects the change in the concentration gradient in the vicinity of the surface. By measuring the dark condition and light condition under the same potential, photocurrent can be observed from the curve. This technique can also be applied to the study of electrode processes mechanisms.

1.4.3.3. Mott-Schottky

Mott-Schottky (M-S) is a classic method for experimentally determining the flatband potential of a semiconductor, which is based on the Mott-Schottky relationship[45]:

$$\frac{1}{C_s^2} = \frac{2}{e\varepsilon\varepsilon_0 A^2 N_D}(V - V_{fb} - \frac{kT}{e})$$

Where C_s is the space-charge capacitance of the semiconductor, ε is the dielectric constant or relative permittivity of the semiconductor, ε_0 is permitivity in vacuum, A is the surface area, e is the charge of an electron, N_D is the free carrier density, k is the Boltzmann constant, T is the temperature, V is the applied potential, and V_{fb} is the flatband potential.

This technique involves measuring the capacitance of the space charge layer of the semiconductor electrode as a function of the applied potential. The flatband potential can be used to determine the energy levels of the conduction and valence band for the semiconductor. The conductivity type is also revealed by M-S analysis. In an n-type semiconductor, the space-charge region is populated by positive charges and the M-S plot will slope downward at more negative potentials. The opposite is true for p-type materials.

In this work, all the linear scanning voltammetry (LSV) measurements were performed on CHP films coated on FTO in the dark, under illumination, and under chopped light from -0.6 V to 2 V vs. Ag/AgCl with a scan rate of 10 mV/s. The electrolyte was 0.02 M Na_3PO_4, either at pH 5, or adjusted to pH 12 with

NaOH. Chronoamperometry (CA) measurements were performed under 1.5 V vs. SCE bias in Na_3PO_4 electrolyte (pH 5) and 0 V vs. SCE bias in deionized water with Fe^{3+} and sodium acetate. The photocurrent was evaluated by subtracting the dark current from the light current. Mott-Schottky (M-S) measurements were performed on CHP coated onto FTO substrates and Au/FTO substrates without light irradiation under a frequency of 100 Hz or 10 Hz. The voltage range was -0.15 to 0.2 V vs. SCE (for samples on FTO) or vs. Ag/AgCl (for samples on Au/FTO substrates), the voltage amplitude was 15 mV, and the equilibration time was 15 minutes. The electrolyte was 0.02 M Na_3PO_4 (pH 5). Photocatalytic oxygen evolution was performed in CHP suspensions with a concentration of 1 g/L under irradiation. Electrochemical water oxidation was performed under dark conditions by applying 1 V vs. Ag/AgCl bias between a Pt counter electrode and CHP coated on FTO. The electrolyte was 0.02 M Na_3PO_4 (pH 12)

2. Experimental Section

2.1. Materials and Reagents

Commercial $Cu_2(OH)PO_4$ powder, acetylacetone, Triton X-100 and $RuCl_3 \cdot 3H_2O$ powder and all the other chemicals were obtained from Sigma-Aldrich and were used without further purification. The fluorine-tin oxide coated glass (FTO) with sheet resistance of 15 Ω/sq was obtained from Hartford Glass Co. De-ionized (DI) water was used in all experiments

2.2. Synthesis of $Cu_2(OH)PO_4$

2.2.1. Hydrothermal Synthesis

2.2.1.1. CuCl and $LiOH \cdot H_2O$ Reactants

$Cu_2(OH)PO_4$ was synthesized through a hydrothermal method using CuCl and $LiOH \cdot H_2O$. The procedure is similar to the method reported by Gopalakrishna et al.[46] and Ji et al.[47]

A number of experiments were carried out using different temperatures and synthesis times in order to study the synthesis process. In a typical procedure, 0.236 g $LiOH \cdot H_2O$, 0.12 g $LiNO_3$ and 0.482 g CuCl were added to 18.75 mL of H_3PO_4 solution (0.1 mol/L). After stirring for 10 min, the mixture was transferred to a Teflon-lined stainless steel autoclave (inner volume: 45 mL) and heated at 170 ℃ for 5 h or 10 h. Heating at 200 ℃ for 2 h, 5 h and 8 h, was also performed. After the hydrothermal reaction, the reactors were cooled to room temperature. The precipitated powder was washed with ethanol. Then, the obtained powder was dried at 50 ℃ in an oven.

2.2.1.2. $CuSO_4 \cdot 5H_2O$ and $CO(NH_2)_2$ Reactants

In this procedure, the reactants were changed to $CuSO_4 \cdot 5H_2O$ and $CO(NH_2)_2$ (urea). Since LiOH is a strong alkali base, once the LiOH and $CuSO_4$ were mixed, a blue precipitate was formed immediately, likely $Cu(OH)_2$. In order to grow $Cu_2(OH)PO_4$ particles directly, a weak base such as $CO(NH_2)_2$ was used. In a typical procedure, 1.25 g $CuSO_4 \cdot 5H_2O$ was added to a 18.75 mL H_3PO4

solution (0.1 mol/L) while 0.5 g $CO(NH_2)_2$ was added to another 18.75 mL H_3PO_4 with same concentration. These solutions were stirred separately and then mixed together until the powders were completely dissolved. Half of the mixed solution (18.75 mL) was transferred to the Teflon-lined stainless steel autoclave and heated at 200 ℃ for 0.5 h, 1 h and 2h or 150 ℃ for 2 h. The reactors were cooled to room temperature. The precipitated powder was washed with ethanol. Then, the obtained powder was dried at 50 ℃ in an oven.

2.2.2. Precipitation Method

$Cu_2(OH)PO_4$ was synthesized using a precipitation method from $CuSO_4 \cdot 5H_2O$ and $LiOH \cdot H_2O$. In this procedure, 0.236 g $LiOH \cdot H_2O$ and 1.25 g $CuSO_4 \cdot 4H_2O$ were added to 18.75 mL H_3PO_4 solution(0.1 mol/L) with 0.2 g/L CTAB (hexadecyltrimethylammonium bromide) dissolved in the solution to serve as surfactant[47]. The mixture was stirred and heated at 100 ℃ on a hot plate which was put in a fume hood for 2 h. After the reaction, it was cooled to room temperature. The precipitated powder was washed with ethanol. Then, the obtained powder was dried at 50 ℃ in an oven.

In another procedure, 0.472 g $LiOH \cdot H_2O$ and 1.25 g $CuSO_4 \cdot 4H_2O$ were added to 37.5 mL H_3PO_4 solution (0.1 mol/L) with 0.2 g/L CTAB dissolved in the solution. The mixture was stirred and heated at 100 ℃ on a hot plate which was put in a fume hood for 2 h. After the reaction, it was cooled to room temperature. The precipitated powder was washed with ethanol. Then, the obtained powder was dried at 50 ℃ in an oven.

XRD was used for obtaining phase identification and structural information. Sample morphology was examined by SEM.

2.3. Characterization

In this work, all X-ray diffraction (XRD) analyses were performed using a high resolution X-ray diffractometer offered by Panalytical X'pert Pro, and monochromatic CuKα radiation was used as the X-ray excitation (λ=1.5405Å). Sample powders were held by a zero background substrate. Each scan started from 10° and ended at 60° or 80° (2θ), with a step size of 0.01 s, scan speed of 0.08 °/s and time per step of 20 s. Scanning electron microscopy (SEM) images were acquired on a FEI XL 30 Environmental FEG, which is also equipped with the EDAX system that can be used to do the energy-dispersive X-ray spectroscopy (EDS) for composition analysis. All the SEM specimens were prepared by a dispersion method in which the sample powders were dispersed in isopropanol through sonication for 15 min. One droplet of the as prepared suspension was then dropped onto a small piece of silicon wafer until the isopropanol was evaporated. UV-vis spectroscopy was with a wavelength range of 250 – 600 nm (Perkin Elmer Lambda 18).

2.4. Preparation of Electrodes

CHP electrodes were fabricated by coating a viscous slurry of the commercial CHP powder on a fluorine-tin oxide (FTO) glass substrate and Au-coated FTO substrates by doctor blading as previous reported by Hiroshi Hashiguchi[48]. The substrates were cleaned by ultrasonication in acetone, ethanol

and deionized water for 30 min each and then dried in air. To make thick films (~ 100 μm) for Mott-Schottky measurements, a CHP slurry was prepared by mixing 0.22 g CHP, 500 μL water, 20 μL acetylacetone, and 10 μL Triton X-100, which served as a surfactant. The slurry was stirred for 2 h, then applied to the substrate using a #3 JR drawdown rod and automatic laboratory drawdown machine (Auto-Draw III). After coating, the samples were calcined at 400 ^{o}C for 2 h to remove the organic solvent and surfactant and to enhance the attachment of CHP powder to the FTO. The CHP slurry was also deposited onto FTO substrates that were coated with Au using sputtering (5 min deposition time). Some of the CHP electrodes were modified by adding 1 % $RuCl_3 \cdot 3H_2O$ in the CHP slurry as a co-catalyst. After calcining, the Ru species converted to RuO_2, which was fully mixed into the CHP film.

Another set of CHP electrodes was fabricated by electrophoretic deposition as reported previously by Ryu Abe[49]. The CHP solution was prepared by dispersing 150 mg CHP in 60 mL acetone through sonication for 15 min. Two as-cleaned FTO electrodes were immersed parallel to each other in the CHP solution with a separation distance of 5 mm. The immersed area was controlled to be 2.97 cm^2. One electrode served as the working electrode while the other was the counter electrode. Application of a 10 V bias between the electrodes was performed using a potentiostat (Biologic VMP3). After electrophoretic deposition, the coated FTO slide was dried by heating at 400 ^{o}C for 2 h. RuO_2 deposition[50] was carried out by loading a small amount of $RuCl_3 \cdot 3H_2O$ solution onto the

surface of the as-prepared CHP electrode. The solution of $RuCl_3 \cdot 3H_2O$ was prepared by dissolving 2 mg $RuCl_3 \cdot 3H_2O$ in 630 µL deionized water, followed by sonication for 10 min. 10 µL of the as-prepared solution was loaded on the CHP electrode using a pipette and then heated at 350 ^oC for 2 h for drying as well as converting the Ru species to RuO_2, which served as a cocatalyst.

To make thinner films, CHP electrodes were fabricated by preparing a homemade CHP paste onto an FTO substrate also using the doctor blading technique. The CHP paste[51] was prepared by adding 10 µL acetic acid to 0.05 g CHP and grinding with a mortar and pestle for 1 min. Then, 50 µL deionized water was added into the mortar followed by grinding for 1 min. This was repeated 3 times. After that, 0.1 mL ethanol was added into the mortar followed by grinding for 1 min. This was repeated 6 times. Finally, 10 µL Triton X-100 was added as a surfactant. The CHP paste was then transferred to a small beaker using 0.3 µL ethanol and sonicated for 15 min. After coating 10 µL of the as-prepared CHP paste onto the FTO substrate, the electrodes were calcined in a programmed oven. The program was set to ramp from 25 ^oC to 450 ^oC at 4 ^oC/min, then kept at 450 ^oC for 30 min, and cooled to 25 ^oC over 2 h.

2.5. Electrochemical and Photoelectrochemical Tests

All photoelectrochemical tests were performed using a 450 W Xe-arc lamp (Newport) at 300 mW/cm^2 light intensity with a water filter. The counter electrode was Pt wire and either a Ag/AgCl or saturated calomel (SCE) electrode was used for the reference electrode. Electrochemical measurements were

performed using a Biologic EC-Lab VMP3 potentiostat. The electrolyte was prepared by dissolving Na_3PO_4 (either 0.02 M or 0.5 M) in deionized water (pH of 5 or 12).

2.5.1. Photocurrent

Slurries of suspended CHP powder (0.5 g/L) were evaluated for photoactivity by using an Fe^{3+} electron transfer mediator (0.5 mM $FeCl_3$) with sodium acetate (0.2 M NaOAc) as the electron donor[52]. The measurement was performed using chronoamperometry (CA). A bias voltage of 0.6 V was applied between the Pt wire working electrode and SCE reference electrode and the subsequent current was measured under dark and illuminated conditions. The pH was adjusted to 5 using acetic acid or NaOH. The flatband potential of CHP was also determined by using methyl viologen[53,54] as a redox mediator and testing for photoactivity at different pH. This measurement was performed by applying -0.4 V vs. Ag/AgCl bias to the Pt wire working electrode, which was immersed in a CHP suspension (0.1 g in 150 mL Na_3PO_4) containing 1.0 mM methyl viologen dichloride, and measuring the current under dark and illuminated conditions. The pH was measured using a Hanna Instruments (HI9125) pH meter.

CHP films on FTO were used for linear scanning voltammetry (LSV), which was performed in the dark, under illumination, and under chopped light from -0.6 V to 2 V vs. Ag/AgCl with a scan rate of 10 mV/s. The electrolyte was 0.02 M Na_3PO_4 (pH 5 or 12). Chronoamperometry (CA) measurements were performed at 1.5 V vs. SCE in Na_3PO_4 electrolyte (pH 5) and 0 V vs. SCE in

deionized water with Fe^{3+} and sodium acetate. The photocurrent was evaluated by subtracting the dark current from the light current.

2.5.2. Mott-Schottky

Mott-Schottky (M-S) analysis[55] were performed on CHP coated onto FTO substrates and Au/FTO substrates without light irradiation using a frequency of 100 Hz or 10 Hz. The voltage range was -0.15 to 0.2 V vs. SCE (for samples on FTO) or vs. Ag/AgCl (for samples on Au/FTO substrates), the voltage amplitude was 15 mV, and the equilibration time was 15 minutes. The electrolyte was 0.02 M Na_3PO_4 (pH 5).

2.5.3. Photocatalytic Oxygen Evolution

CHP powder was suspended in 130 mL deionized water at a concentration of 1 g/L in a custom-made photochemical cell with a Teflon cap that provided an air-tight seal. The cell also had a quartz window to allow for the UV-light from the 450 W Xe-arc lamp to be absorbed by the CHP. Prior to irradiation, the solution was purged with Ar for 1 h to remove the air. The oxygen concentrations were recorded using a phase fluorescence-based sensor patch (Neofox, with FOXY coated RedEye patch sensor, Ocean Optics) with the sensor above the solution. This technique has been used in other water oxidation studies to quantify the amount of produced O_2 [56,57].

2.5.4. Electrocatalytic Water Oxidation

Electrolysis under dark conditions was performed by applying 1 V vs. Ag/AgCl between a Pt counter electrode and CHP coated on FTO (6.912 cm^2). The measurement was performed in a custom-made photochemical cell with electrical connections fed through air-tight septa. The electrolyte (0.02 M Na_3PO_4, pH 12) was purged with Ar for 1 h prior to the measurement and oxygen concentrations were recorded using fluorometry with the sensor immersed in the electrolyte. A bare FTO slide with the same immersed area was also measured as a control.

3. Results and Discussion

3.1. Structure and Morphology of Commercial CHP

CHP crystalizes in an orthorhombic structure with space group Pnnm and lattice constants a = 8.062, b = 8.384, c = 5.881 [52,58] as confirmed by X-ray diffraction of the commercial CHP powder (Aldrich) without impurities(Fig. 2). The structure of CHP consists of $Cu_2O_6(OH)_2$ dimers and 1-dimensional $Cu_2O_6(OH)_2$ chains linked by PO_4 tetrahedra. The bridging hydroxyl group is a unique feature of the CHP structure and is thought to be the source of highly active hydroxyl radicals that impart catalytic activity to CHP. CHP was observed to decompose when films were annealed in air at temperatures greater than 500 ^oC. XRD measurements showed the presence of some new peaks after annealing at

550 ^{o}C and annealing at 700 ^{o}C showed partial transformation of CHP to $Cu(HPO_3)(H_2O)_2$ (Fig. 3). This is consistent with reports on the dehydration of CHP to $Cu_4(PO_4)_2O$ at temperatures above 500 ^{o}C [59].

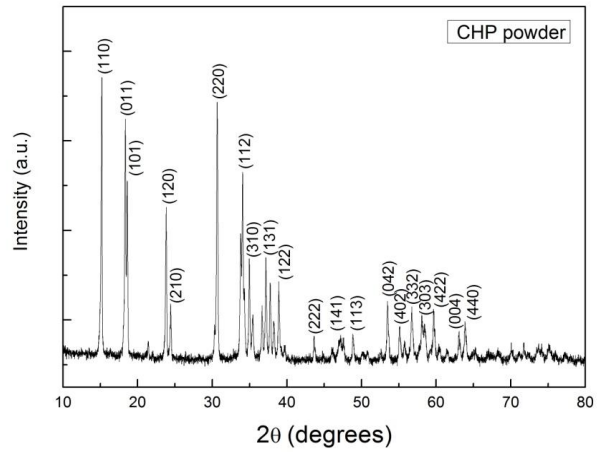

Figure 2. XRD pattern of the commercially obtained CHP

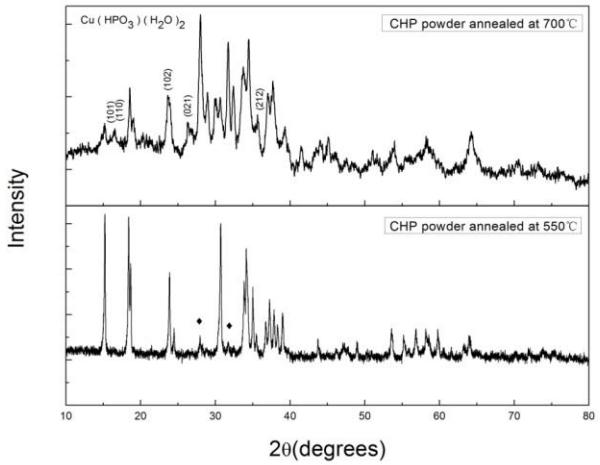

Figure 3. XRD pattern showing CHP annealed at 500 ^{o}C and 700 ^{o}C

The SEM image of the commercially obtained CHP revealed particles with rod-like morphologies with lengths of ~1 micron and diameters of 100-500 nm

(Fig. 4). The commercial CHP was a light green powder. All the other measurements on investigating the photoelectrochemical and electrochemical properties of CHP were done on commercial CHP in order to obtain uniform results.

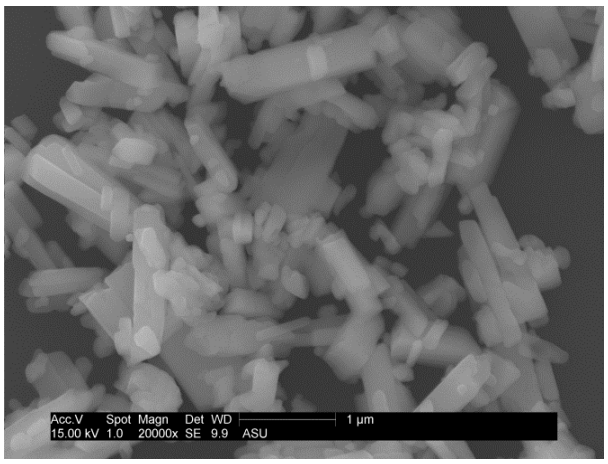

Figure 4. SEM image of commercially obtained CHP

3.2. Structure and Morphology of Synthesized CHP

3.2.1. Hydrothermal Synthesis using CuCl and LiOH • H_2O Reactants

The product synthesized from CuCl and LiOH • H_2O using hydrothermal treatment at 170 ℃ was a mixture containing reddish powders and dark green powders. The pH before the reaction was 5~6. Comparing the products obtained from reaction at 170 ℃ for 5 h (CuCl-1) and 10 h (CuCl-2), mostly reddish powders and a few dark green crystal powders were observed in sample CuCl-1 while sample CuCl-2 had more dark green powders mixed with fewer reddish powders. XRD of CuCl-2 (Fig. 5) matched the CHP pattern well while several

peaks were attributed to Cu_2O (Fig. 6) and residual CuCl (Fig. 7). The intensity of the characteristic peaks of CHP in CuCl-1 was not as strong as in CuCl-2 while some stronger peaks matched CuCl and Cu_2O (Fig. 8). This indicates that for the 170 ℃ synthesis, a longer reaction time was better for converting CuCl and Cu_2O to CHP. The SEM image of CuCl-1 showed a few large particles ~10 μm in size with a prism morphology (Fig. 9) and some small particles aggregated together (Fig. 10). The prism is bounded with four trapezoid prism faces and four trigonal end caps, which also been reported by Xu et. al. [60] using $CuCl_2$ and $(NH_4)_2HPO_4$ as reactants. SEM images of CuCl-2 showed a similar morphology but with more large particles (Fig. 11) and less small particles. This suggests that the large prism particles are CHP while the small particles are CuCl or Cu_2O.

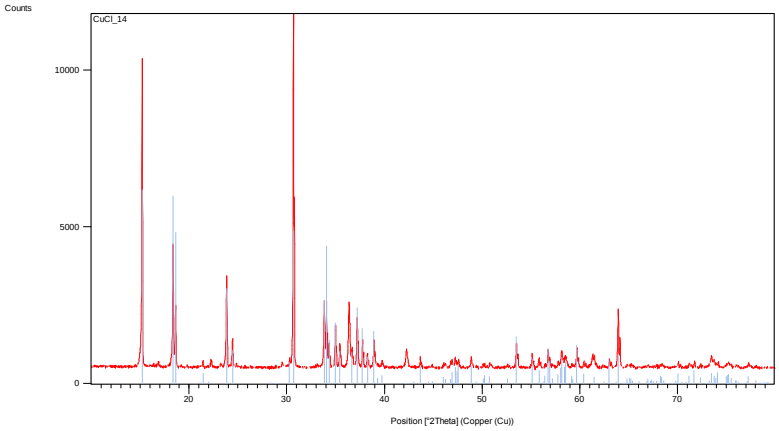

Figure 5. XRD result confirmed the formation of CHP (blue lines) for sample CuCl-2

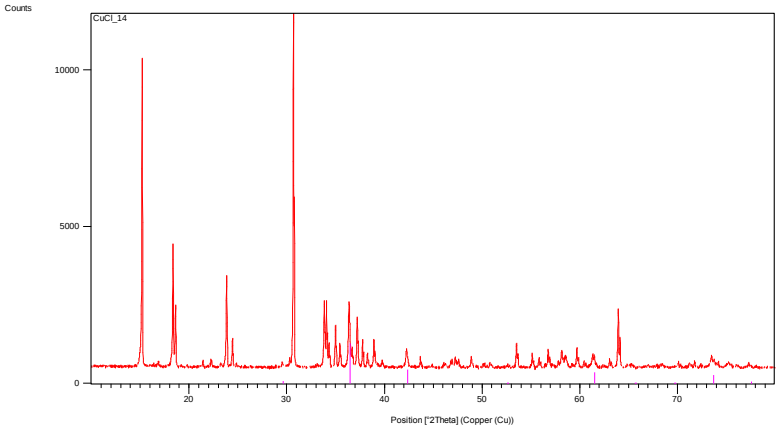

Figure 6. XRD result of sample CuCl-2 compared with Cu_2O (red lines)

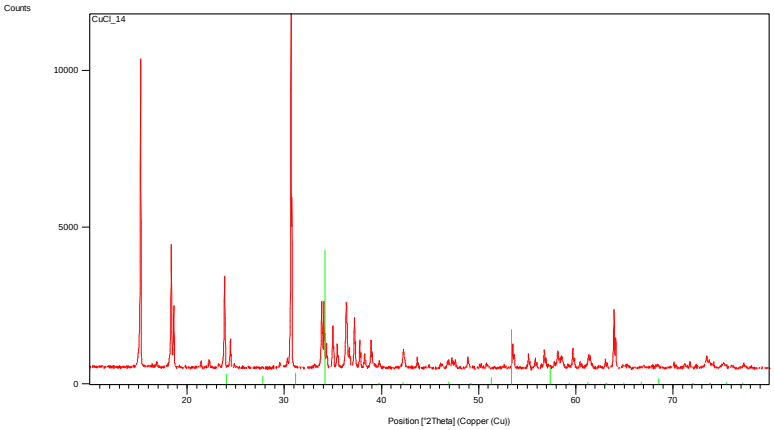

Figure 7. XRD result of sample CuCl-2 compared with CuCl (green lines)

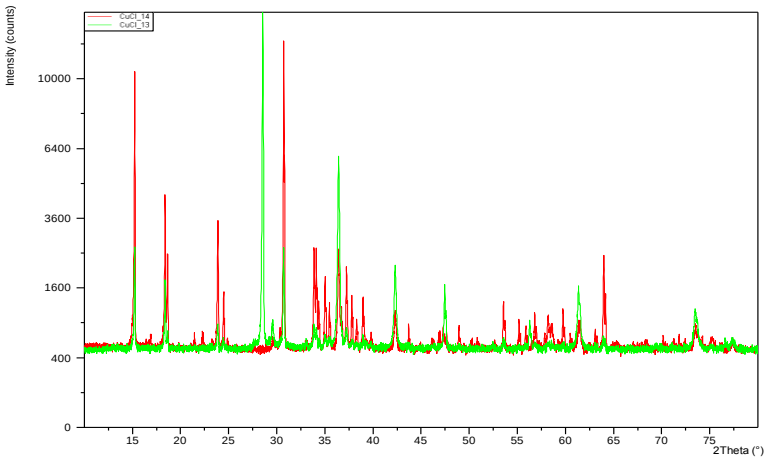

Figure 8. Comparison of XRD results for sample CuCl-1(green pattern) and CuCl-2 (red pattern)

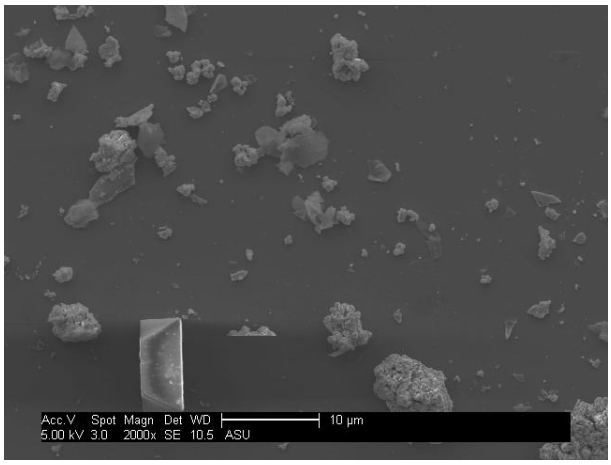

Figure 9. SEM image of CuCl-1 (2000x)

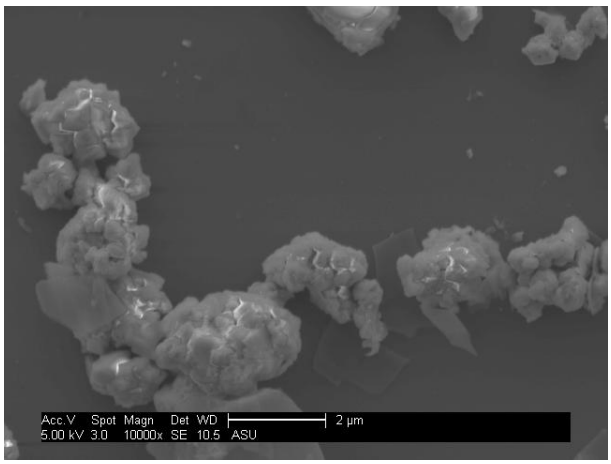

Figure 10. SEM image of CuCl-1 (10000x)

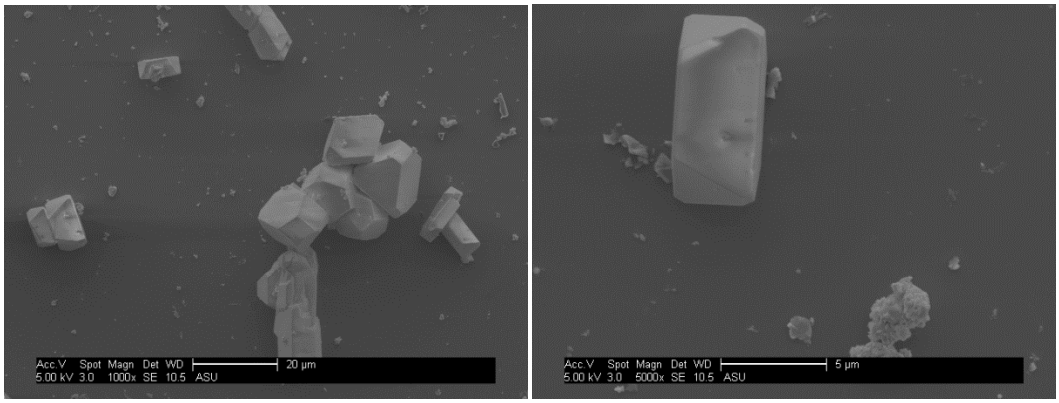

(a) (b)

Figure 11. SEM image of CuCl-2 1000x (a) and 5000x (b)

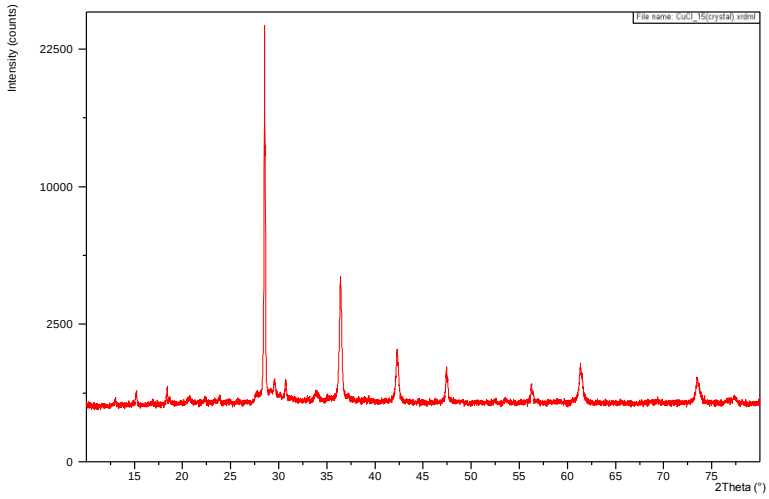

Figure 12. XRD result of sample CuCl-3

The reaction temperature was increased to 200 ℃ for 2 h (CuCl-3), 5 h (CuCl-4) and 8 h (CuCl-5). Only reddish powders were observed in sample CuCl-3. Samples CuCl-4 and CuCl-5 consisted of a mixture of reddish powders and dark green crystal powders, but there were more green powders in CuCl-5 than in CuCl-4. Fig. 12 is the XRD of CuCl-3, which showed no CHP pattern. By separating the reddish powders and dark green powders in CuCl-4 and CuCl-5, XRD could be used to attempt to identify each type of powder. Fig. 13 compares

the XRD pattern of the CuCl-4 green powders and reddish powders. It can be seen clearly that the green powers are CHP while the reddish power contains some other peaks of Cu_2O (Fig. 14). XRD of the CuCl-5 green powders (Fig. 15) also matches the CHP pattern quite well. SEM of CuCl-3 (Fig. 16) showed a powder morphology similar to that found in CuCl-1, which was mostly small particles and a few prism particles about ~5 μm. There are fewer and smaller-sized prism particles compared to CuCl-1, which explains why there is no obvious CHP

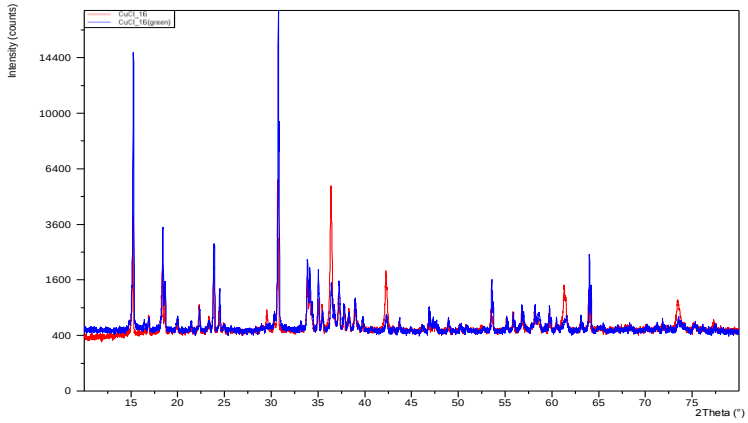

Figure 13. XRD results comparing the CuCl-4 green powders (blue pattern) and reddish powders(red pattern)

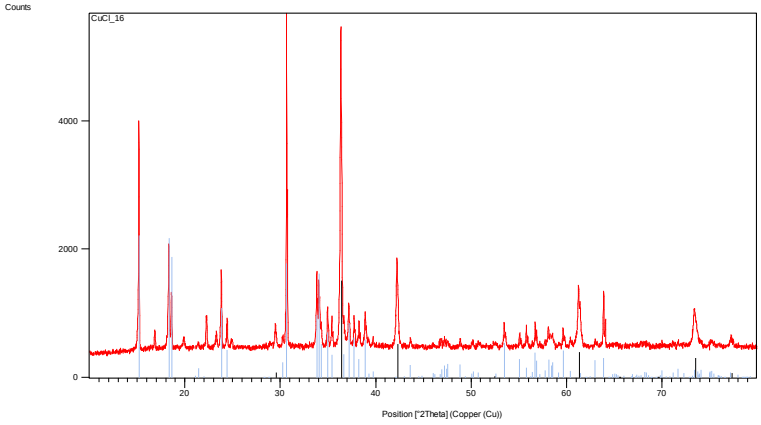

Figure 14. XRD results of the CuCl-4 reddish powders confirming presence of CHP (blue lines) and Cu_2O (black lines)

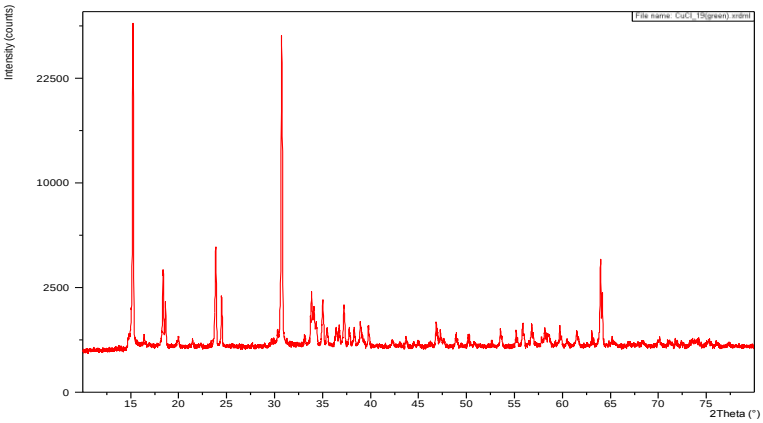

Figure 15. XRD result of the CuCl-5 green powders

pattern observed in the XRD of CuCl-3. SEM images of CuCl-4 and CuCl-5 green powders showed a similar morphology, of mostly large particles (Fig. 17) even larger than ~20 μm and a few aggregated small particles (Fig. 18), probably because the separation into green and red powders was not exact. The results also indicate that for 200 ℃ hydrothermal synthesis, a long reaction time is better for converting CuCl and Cu_2O to CHP. But even by increasing the temperature and reaction time, Cu_2O was always observed mixed in the product. Since it is easy for CuCl to become Cu_2O once dissolved in water, but hard to convert Cu_2O to CHP, CuCl is not a good reactant to use in the synthesis of CHP.

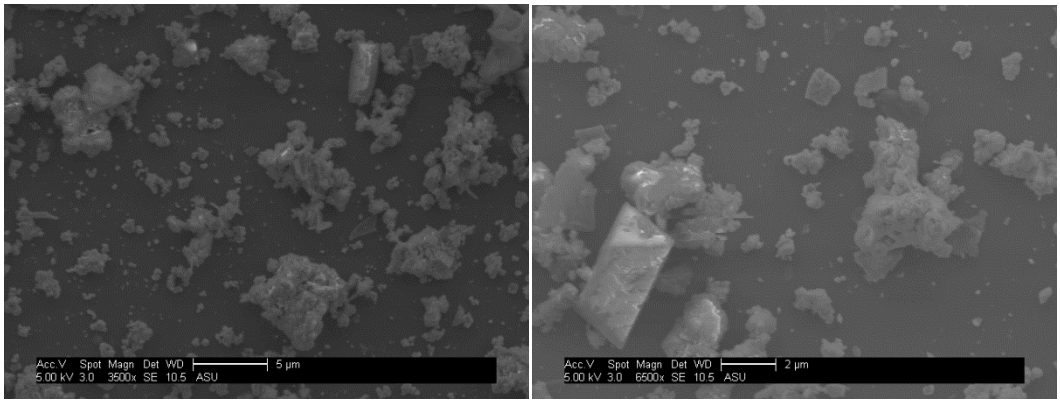

(a) (b

Figure 16. SEM image of CuCl-3 3500x (a) and 6500x (b)

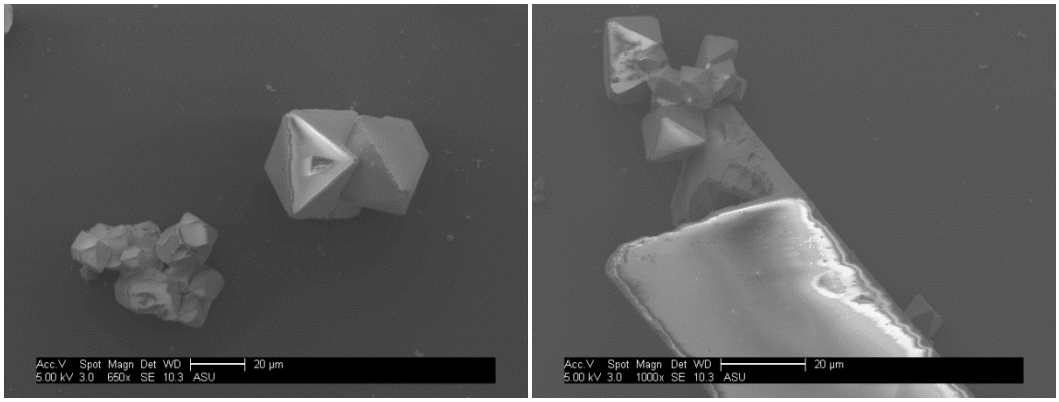

(a) (b)

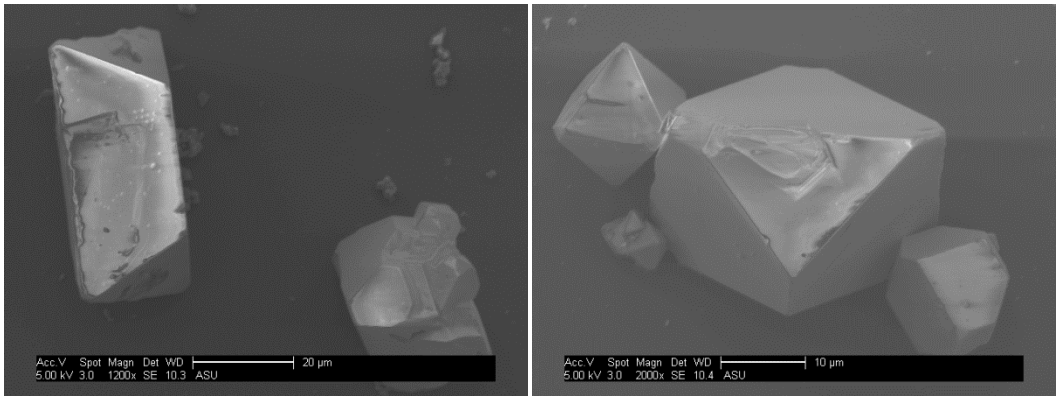

(c) (d)

Figure 17. SEM image of large green particles of CuCl-4 650x (a), 1000x (b), 1200x (c) and 2000x (d)

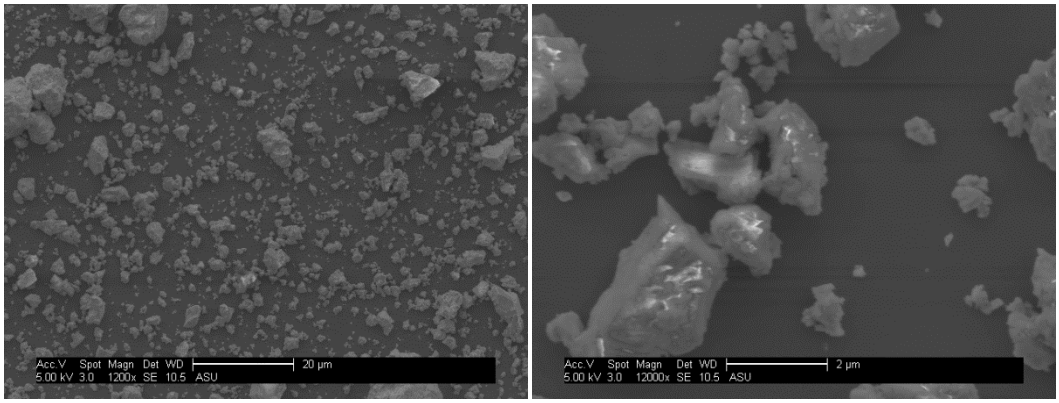

(a) (b)

Figure 18. SEM image of small green particles of CuCl-5 1200x (a) and 12000x (b)

3.2.2. CHP Synthesis using $CuSO_4$ as Reactant

3.2.2.1. Hydrothermal Synthesis using $CuSO_4 \cdot 5H_2O$ and $CO(NH_2)_2$

For hydrothermal synthesis performed at 200 ℃, a mixture of blue powders and dark green powders were observed in samples reacted for 30 min (Cu-1) and 1 h (Cu-2). For samples reacted for 2 h (Cu-3), only dark green crystal powders were observed. The large amorphous halo in the XRD pattern of Cu-1 and Cu-2 indicated that the blue powders of the as-synthesized products are low in crystallinity (Fig. 19). No obvious CHP pattern was observed. XRD of Cu-3 and the dark green powders from Cu-1 and Cu-2 matched with the CHP pattern quite well (Fig. 20), which indicates that 30 min and 1 h are not enough to synthesize pure CHP. SEM images of Cu-3 (Fig. 21) and the green powders of Cu-1 (Fig. 22 (a)) and Cu-2 (Fig. 23 (a)) show large particles ~50-100 μm while the blue powders of Cu-1 and Cu-2 are mostly small particles (Fig. 24). The

particle size of Cu-3 is a little bit larger than Cu-1 and Cu-2, in which several prism particles were observed (Fig. 22 (b) & 23 (b)). This probably indicates that the prism particles formed first and as the reaction time increased, they aggregated to form larger, irregular particles.

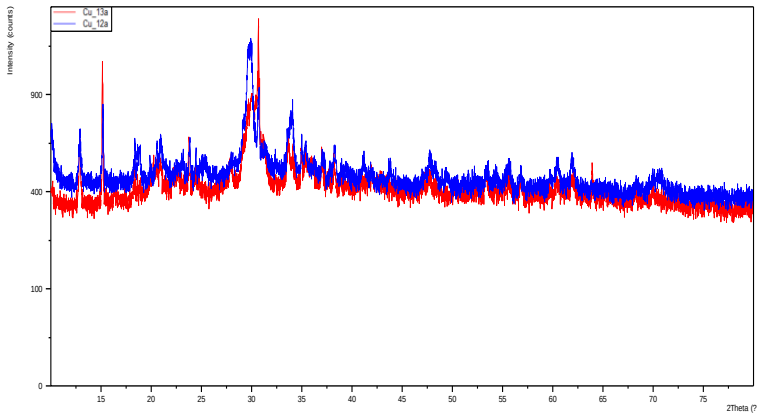

Figure 19. XRD results of blue powders from Cu-1 (blue pattern) and Cu-2 (red pattern)

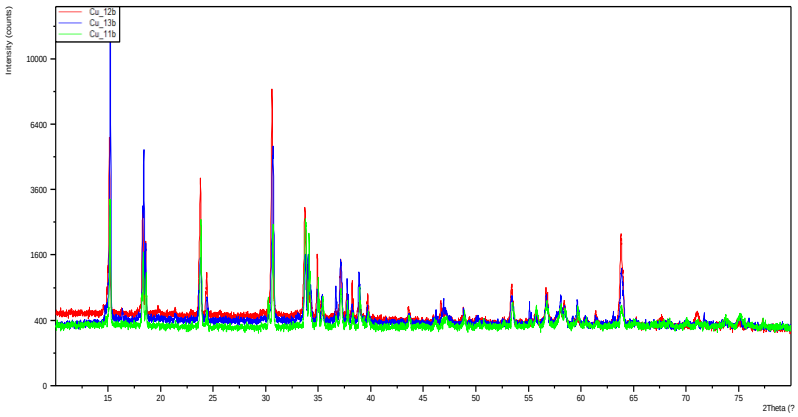

Figure 20. XRD results of dark green powders from Cu-1 (red pattern) and Cu-2 (blue pattern) and Cu-3 (green pattern)

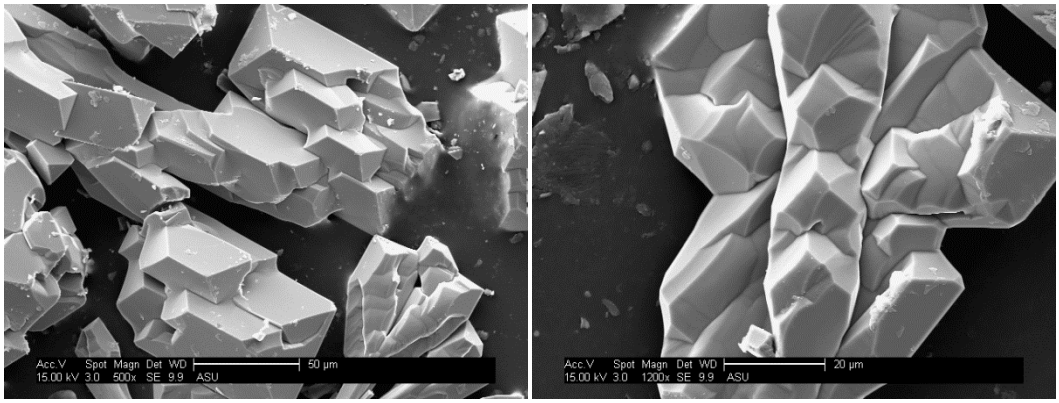

(a) (b)

Figure 21. SEM image of Cu-3 500x (a) and 1200x (b)

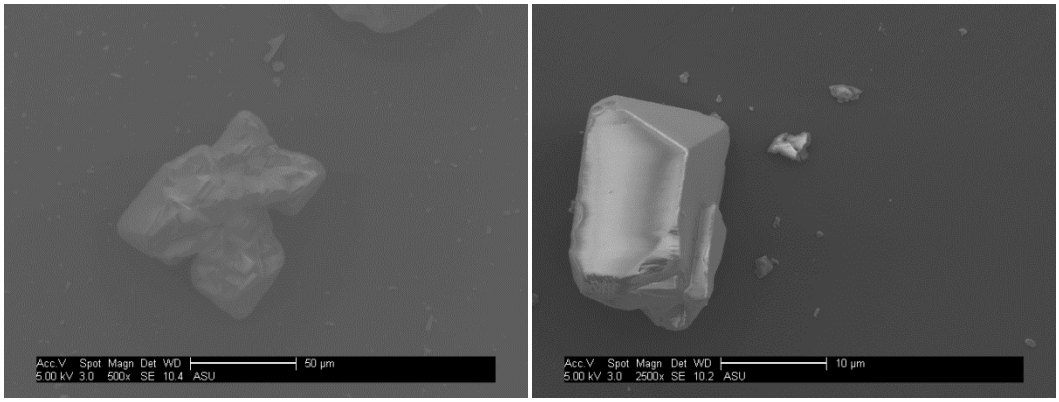

(a) (b)

Figure 22. SEM image of green powders of Cu-1 500x (a) and 2500x (b)

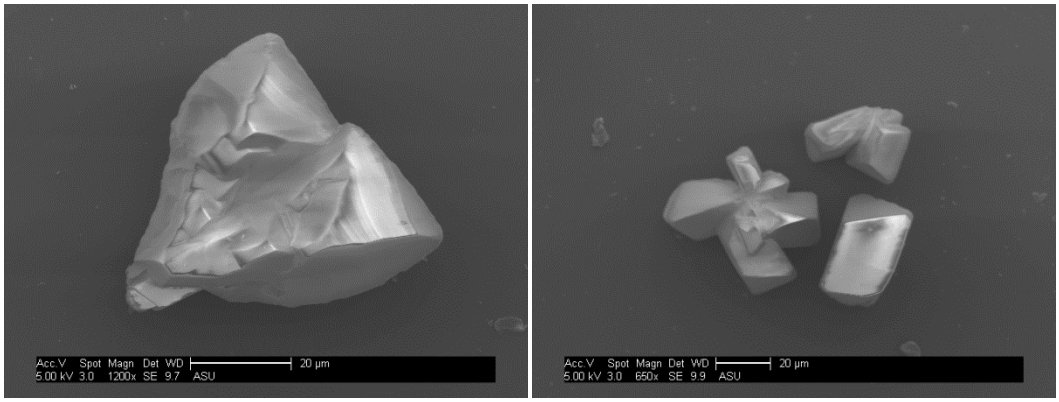

(a) (b)

Figure 23. SEM image of green powders of Cu-2 1200x (a) and 650x (b)

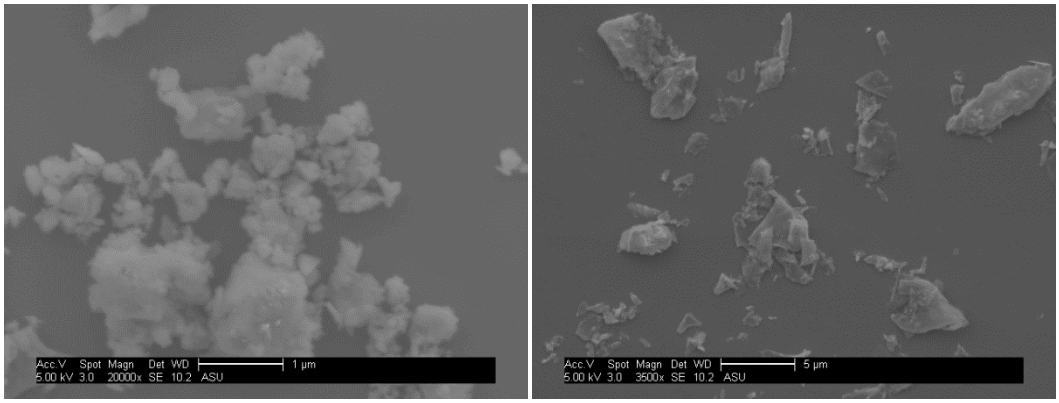

(a) (b)

Figure 24. SEM image of blue powders of Cu-1 20000x (a) and Cu-2 3500x (b)

To determine if a lower temperature can result in smaller CHP particles, the sample Cu-3, which was reacted at 200 ℃ for 2h, was compared with the product reacted at 150 ℃ for 2 h (Cu-4). However, the product of Cu-4 was still a mixture of blue and dark green particles. By comparing XRD of the Cu-4 blue powders and dark green powders (Fig. 25), the blue powder also showed a similar pattern to CHP, just with weak intensity, which probably is because the product was not precisely separated into green powder and blue powder. Also this may indicate that in the synthesis process, the blue amorphous phase formed first and then transformed into CHP, the green powder. This is consistent with the report on formation of amorphous spherical nanoparticles after 10 min reaction of the $Cu(NO_3)_2 \cdot 3H_2O$ solution and the $(NH_4)_2HPO_4$ solution[1]. The SEM image of the dark green powders from Cu-4 (Fig. 26) showed similar irregular large particles to Cu-1, Cu-2, and Cu-3.

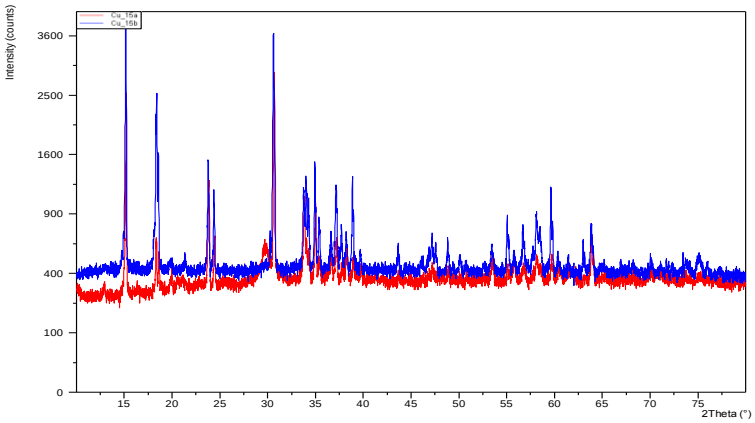

Figure 25. XRD results of Cu-4 blue powders (red pattern) and dark green powders (blue pattern)

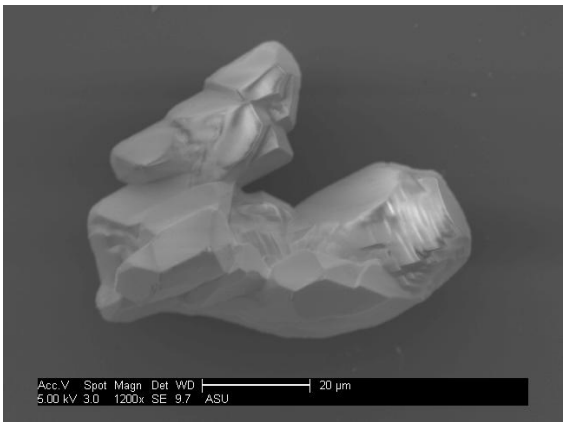

Figure 26. SEM image of Cu-4 dark green powders

3.2.2.2. Precipitation Method using $CuSO_4 \cdot 5H_2O$ and $LiOH \cdot H_2O$

The pH of the solution (Cu-5) with reactants of 0.236 g $LiOH \cdot H_2O$ and 1.25 g $CuSO_4 \cdot 5H_2O$ before reaction was 2~3 while the other one (Cu-6) was 5~6. By comparing these two samples, the effect of pH could be investigated. Both of the products were light green powders (the same color as the commercial CHP) and XRD matched the CHP pattern quite well (Fig. 27). The intensity of

Cu-5 was stronger indicating that a lower reaction pH could lead to better crystallinity of the product. SEM of Cu-5 (Fig. 28) showed a rod-like morphology with a small particle size about ~5 μm in length. Careful observation of the morphology of Cu-5 displayed a split in the end of the rod particle. SEM of Cu-6 (Fig. 29 (a)) showed a similar particle size but with more severe splitting. In order to see the morphology more clearly, high magnification SEM was done for Cu-6. As shown in Fig. 29 (b), a hyperbranched structure was observed. This indicates that the reaction pH has a large effect on the morphology, and that by increasing the pH to 5~6, CHP can be synthesized with a hyperbranched structure.

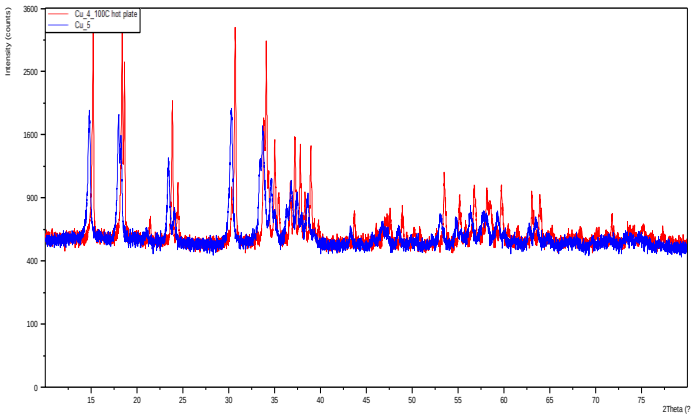

Figure 27. XRD results of Cu-5 (red pattern) and Cu-6 (blue pattern)

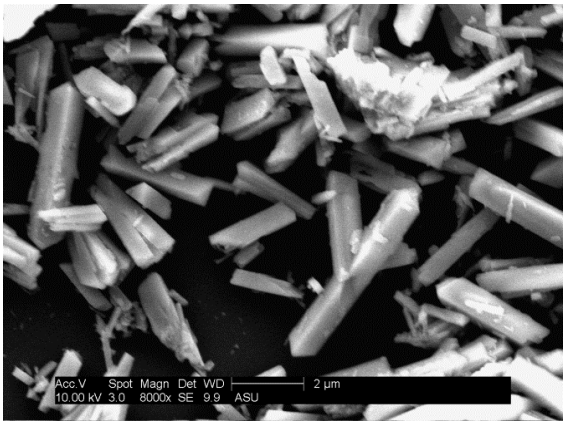

Figure 28. SEM image of Cu-5 8000x

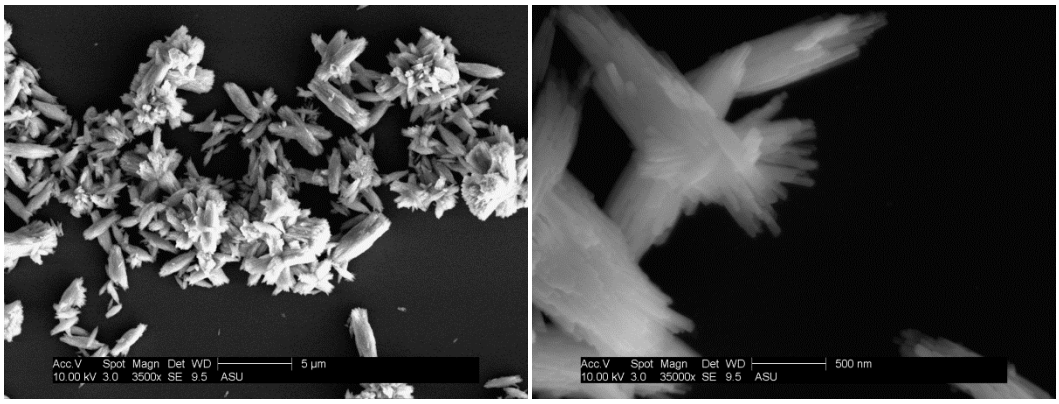

(a) (b)

Figure 29. SEM image of Cu-6 3500x (a) and 35000x (b)

From these experiments, it can be concluded that $CuSO_4$ is a better reactant than CuCl for the synthesis of pure CHP, which can be obtained at 200 ℃ for 2 h. The particle size cannot be adjusted by lowering the reaction temperature since the amorphous blue phase which formed first cannot convert to CHP completely at lower temperatures. By comparing the hydrothermal synthesis and precipitation methods using $CuSO_4$ as reactant, it is clear that the precipitation method is better to synthesize CHP under lower temperatures and the CHP particles are more uniform probably because of stirring while reaction.

3.3. Flatband Potential and Bandgap

Mott-Schottky (M-S) measurements were performed on CHP deposited on FTO and Au-coated FTO substrates, as well as on each substrate without CHP coating as a control. The flatband potential (V_{fb}) of CHP was obtained from the M-S data, which is the intercept of M-S plots[45]. In the case of the Au-coated FTO, the M-S plot did not show any space charge capacitance, consistent with the fact

that the Au is metallic and the FTO was completely isolated from the electrolyte (Fig. 30). A linear region with a positive slope was observed for the CHP films coated on the Au-FTO substrates. Extrapolation of the linear region to the x-axis gave a V_{fb} of 0.004 V vs. Ag/AgCl at 100 Hz and 0.023 V vs. Ag/AgCl at 10 Hz in the pH 5 electrolyte, shown in Fig. 30. A small frequency-dependent behavior in M-S measurements is often observed in non-single crystal substrates and is usually attributed to surface states and structural irregularities on the surface[55,61]. For the CHP films coated on FTO substrate, a similar capacitance response was observed except the V_{fb} were more negative by about 30-50 mV. The V_{fb} determined for the CHP on uncoated FTO was -0.087 V vs. SCE (-0.042 V vs. Ag/AgCl) at 100 Hz (Fig. 31 (a)) and -0.054 V vs. SCE (-0.009 V vs. Ag/AgCl) at 10 Hz in the pH 5 electrolyte (Fig. 31 (b)). The M-S plot for the FTO alone also showed a linear region with positive slope, which is consistent with the fact that SnO_2 is an n-type semiconductor[62]. The V_{fb} determined for the uncoated FTO was -0.159 V vs. SCE (-0.114 V vs. Ag/AgCl) at 100 Hz and -0.104 V vs. SCE (-0.059 V vs. Ag/AgCl) at 10 Hz, also shown in Figure 31. The observed capacitance for the CHP films coated on FTO may be partially contributed by FTO that was exposed to the electrolyte, which may explain the more negative V_{fb} compared to those obtained for the CHP on Au.

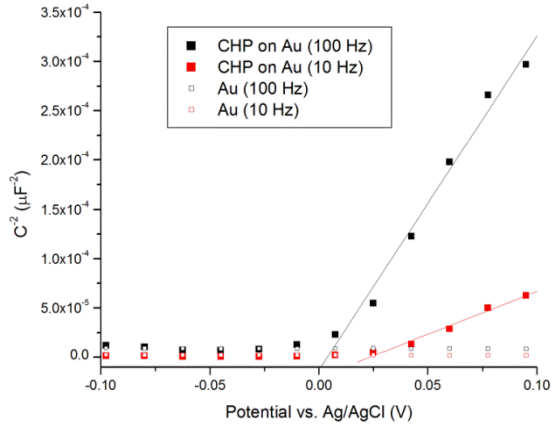

Figure 30. Mott-Schottky plots of CHP coated onto Au-coated FTO compared to bare Au-coated FTO at 100 Hz and 10 Hz

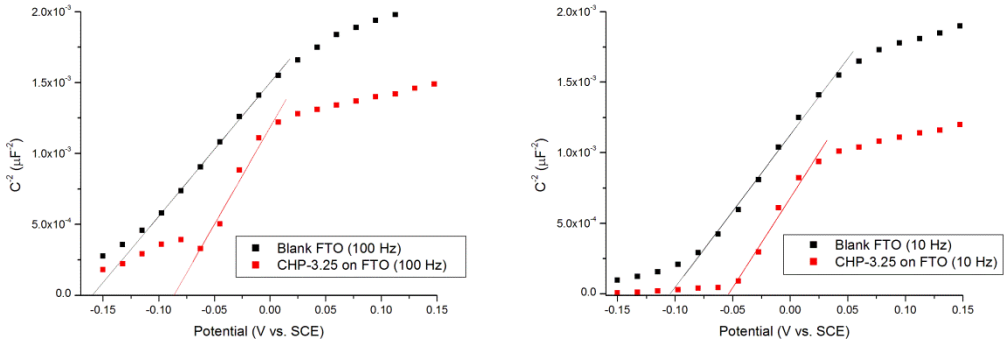

(a) (b)

Figure 31. Mott-Schottky plots of CHP coated onto FTO compared to bare FTO at 100 Hz (a) and 10 Hz (b)

The bandgap (E_g) of CHP was determined using a diffuse reflectance measurement. The reflectance R vs. wavelength is measured using a UV-vis spectrometer and the Kubelka-Munk theory of reflectance can be used to extract absorbtion[63-65]. The value of the band gap in the absorption spectrum was acquired by extrapolating the Tauc plots[66-68] to the baseline. The intersection of

the two lines can be estimated as the band gap of CHP, as shown in Figure 32, which was determined to be indirect bandgap of 3.43 eV. Some examples in the literature point to a morphology and size-dependence on the bandgap for libethenite; a decreasing bandgap was observed with decreasing particle size, with a 0.4 eV bandgap difference as the materials changed from a microrod morphology 10-20 μm in size (Eg = 3.2 eV) to nanostructures 50-300 nm in size (Eg= 2.88 eV) [1,2]. The reason for this observation was not explained, but it is reasonable to suppose that surface states may play a role.

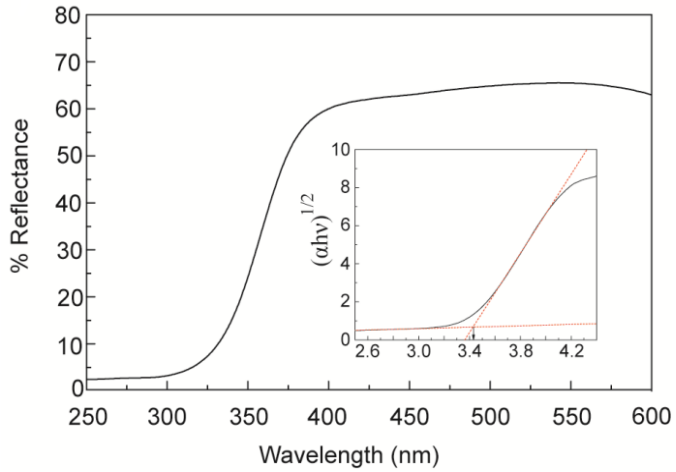

Figure 32. Diffuse reflectance and Tauc plot (inset) for CHP

3.4. Photocurrent

The photoactivity of an aqueous catalyst suspension can be evaluated using an $Fe^{2+/3+}$ redox electron shuttle[52,69], provided the conduction band edge of the semiconductor photocatalyst is higher than the redox potential (E^0 = +0.77 V vs. NHE), which is indeed the case for CHP based on the measured flatband potential. Upon illumination, photogenerated electrons will be transferred from

the conduction band of CHP to reduce Fe^{3+} to Fe^{2+}. The Fe^{2+} species are re-oxidized and the electrons are collected at the Pt collector (working) electrode, creating a measureable photocurrent (Fig. 33 (a), inset). Sodium acetate (NaOAc) was used as an hole scavenger (electron donor) to avoid recombination of the photogenerated carriers. The acetate will become oxidized by photogenerated holes from the valence band of CHP. The oxidation product can be acetate radical ($\cdot CH_2COOH$) which does not react with Fe^{2+} [52], or methyl radical ($\cdot CH_3$) plus CO_2 [70]. Unlike other hole scavengers such as formate and oxalate, there is no current doubling effect with acetate[71]. As shown in Figure 33 (a), a noticeable photocurrent was observed when the light was turned on, and it decreased when the light was turned off. The magnitude of the photocurrent was around 1 $\mu A/cm^2$, but this may be due to the low surface area of the Pt wire used as the collector electrode. Prior studies using this same method on TiO_2 suspensions also showed similar low photocurrents at short irradiation times[69,72]. CA measurements of CHP films on FTO also showed similar behavior when immersed in a solution of 0.5 mM $FeCl_3$ and measured under dark and light conditions without a voltage bias (Fig. 33 (b)). The photocurrent was slightly lower when NaOAc was added as a hole scavenger. The reason for this is not yet understood, since it was expected that presence of NaOAc would improve charge separation. Moreover, the anodic reaction for the case where only $FeCl_3$ was present in the electrolyte was not clear. Nonetheless, these results indicate that photoexcited carriers can be separated and transported to the CHP/electrolyte interface, both when the material is in suspension form and as an electrode.

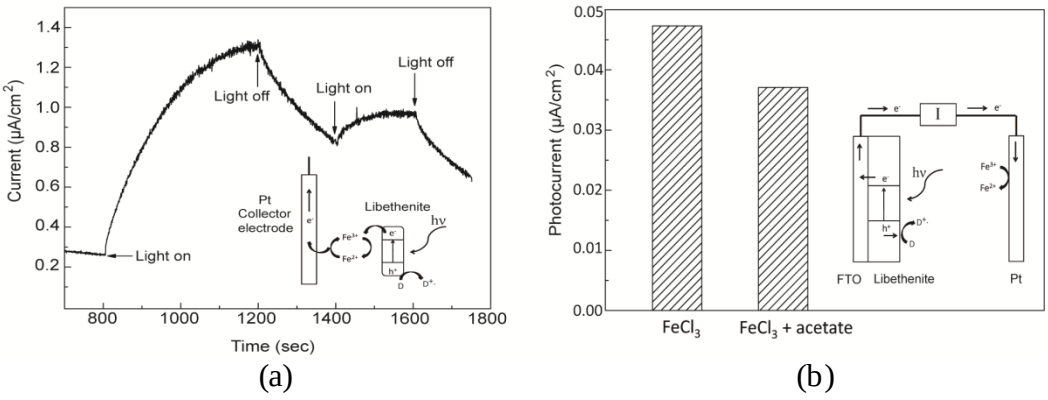

(a) (b)

Figure 33. CA measurements on libethenite (insets illustrate measurement setup)
(a) Libethenite particles suspended in 0.5 mM $FeCl_3$ and 0.2 M NaOAc (electron donor, D) with 0.6 V applied between collector electrode and working electrode
(b) Photocurrent observed from CA on libethenite coated onto FTO and immersed in 0.5 mM $FeCl_3$ only or 0.5 mM $FeCl_3$ and 0.2 M NaOAc with 0 V bias

By performing a similar measurement but replacing the $Fe^{2+/3+}$ redox couple with methyl viologen (MV^{2+}), the V_{fb} of an aqueous catalyst suspension can be determined[53,54]. The advantage of this technique compared to the Mott-Schottky measurement is that any substrate contributions are eliminated. The redox potential of $MV^{2+}/MV^{+}\cdot$ is -0.446 V vs. NHE and is pH independent, while the band energetics of semiconductors will vary with pH due to interactions with H^+ or OH^- in the electrolyte. Upon illumination, photogenerated electrons from the semiconductor will reduce MV^{2+} to $MV^{+}\cdot$ if the suspension pH is high enough for the conduction band of CHP to be more negative than the reduction potential for MV^{2+}. The measured photocurrent arises from the re-oxidation of $MV^{+}\cdot$ species at the Pt collector electrode. Based on the fairly positive V_{fb}

determined with M-S, alkaline suspensions were prepared using 0.1 M Na_3PO_4 with the pH adjusted between 12-13 with NaOH. As shown in Figure 34, no photoresponse was observed at pH 12 or 12.28, but approximately 20 $\mu A/cm^2$ of photocurrent was observed at pH 12.55. At pH 12.82, about 40 $\mu A/cm^2$ photocurrent was observed. The V_{fb}, or more accurately, the quasi-Fermi level for electrons under irradiation, E_F can be determined using the following equation[53]:

$$E_F = E_{redox} + 0.059pH_0$$

where E_{redox} is the reduction potential for $MV^{2+/}MV^{+}\cdot$ and pH_0 is the pH where electron transfer from the semiconductor conduction band to MV^{2+} begins. Taking pH_0 to be 12.55, this gives a E_F of 0.294 V vs. NHE (pH 0) for CHP. The difference from the V_{fb} values determined using M-S may be explained by substrate effects (e.g. FTO contribution, adhesion problems) and the non-ideal nature (e.g. polycrystalline, high surface roughness) of the films. However, the V_{fb} measurements from these two measurements are in good agreement. The energy band diagram of CHP (Fig. 35) was determined by averaging the V_{fb} obtained at the two frequencies used in M-S measurements and also obtained from MV test. The conduction band minimum (E_{cb}) was approximated to be 0.2 eV higher, a typical value for the difference E_{cb}-V_{fb} for n-type semiconductors [73,74]. The location of the valence band with respect to the conduction band was determined using the measured optical bandgap, shown in Figure 32. The location of the band edges indicate that CHP cannot be used as a photocatalyst for overall watersplitting without applying a voltage bias to shift the conduction band

minimum above that potential for H_2 evolution (H^+/H_2 = 0 V vs. NHE, pH 0). However, CHP does have enough overpotential to act as a photocatalyst for water oxidation in the presence of a sacrificial electron scavenger (much like Ag_3PO_4)[39] or as photoanode in a tandem cell Z-scheme configuration (much like WO_3)[32].

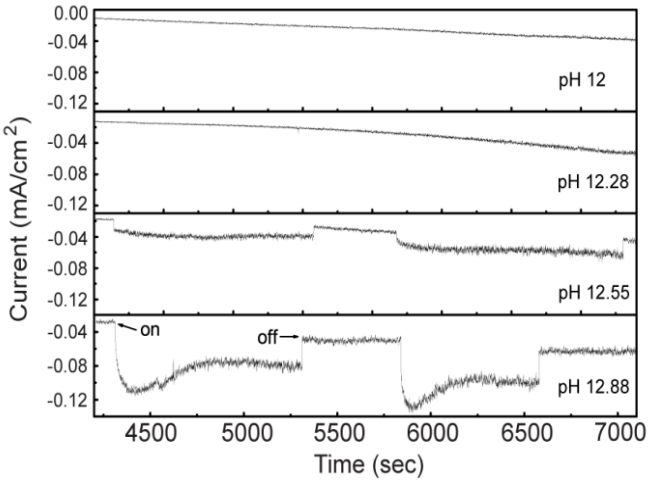

Figure 34. Methyl viologen (MV^{2+}) mediated photocurrent collected on a Pt electrode in suspensions of CHP. A voltage bias of -0.4 V vs. Ag/AgCl was used for MV^{2+}

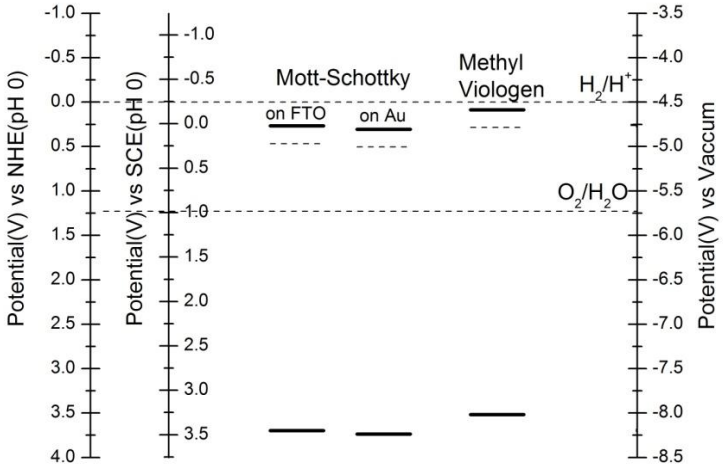

Figure 35. Location of conduction and valence band edges and flatband potentials for CHP as determined by Mott-Schottky (MS) measurements on FTO or Au-coated FTO substrates, by methyl viologen (MV^{2+}) mediated photocurrent measurements

3.5. Photoelectrochemical Properties

In order to understand the photoelectrochemical properties of CHP, chronoamperometry (CA) measurements were performed (Fig. 36). In all cases, the working electrode was held at 1.5 V vs. SCE and the base electrolyte was 0.02 M Na_3PO_4 (pH 5). The average photocurrents observed in the CA measurements is plotted in Figure 37. The CA measurement for CHP deposited onto FTO using electrophoretic deposition (EPD) is shown in sample (1) in Fig. 36, with an average photocurrent of 10 $\mu A/cm^2$. Adding RuO_2, a highly active electrocatalyst for water oxidation[75], was observed to increase the photocurrent, as shown in samples (2) and (3). Coating the RuO_2 on the surface of the CHP increased the photocurrent to 24.6 $\mu A/cm^2$. However, sample (3) shows a much higher photocurrent of 39 $\mu A/cm^2$, which indicates that mixing RuO_2 into the CHP film and depositing it as a slurry is better than coating RuO_2 onto the CHP film surface. It may because mixing RuO_2 together with CHP will make RuO_2 fully coated around CHP powders instead of only touching the surface of the CHP film. The non-square shape of the CA curve for (3) indicates a delayed photoresponse, which may be due to RuO_2 being in the bulk of the film. To better investigate the effect of RuO_2, CA measurements were also performed on samples (1) and (2) under different applied voltages. A noticeable increase was observed by comparing sample (2) with coated RuO_2 on the surface to sample (1), which did not have RuO_2 coating (Fig. 38).

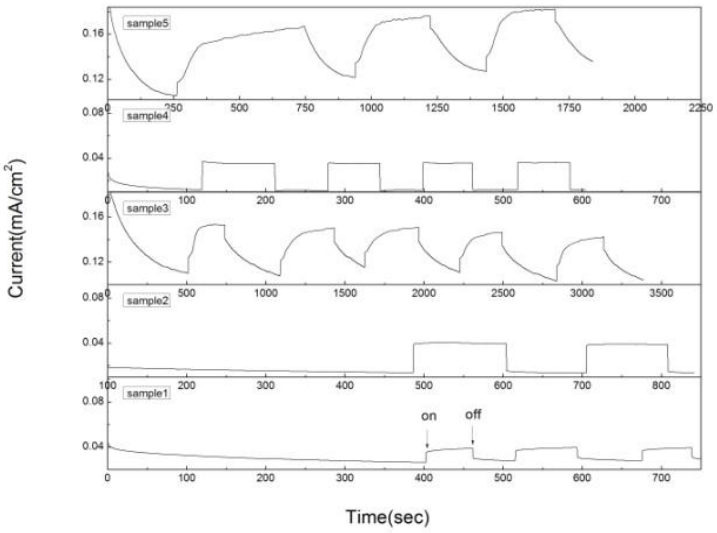

Figure 36. CA measurements of CHP on FTO in 0.02 M Na_3PO_4 with 1.5 V vs. SCE applied bias: (1) Deposited using EPD; (2) Deposited using EPD, followed by decoration with $RuCl_3$ and annealing; (3) Deposited by coating a slurry of libethenite and $RuCl_3$ folllowed by annealing; (4) Deposited using EPD, added 10 vol% MeOH as hole scavenger; (5) Deposited using EPD, added 0.075 vol% H_2O_2 as hole scavenger

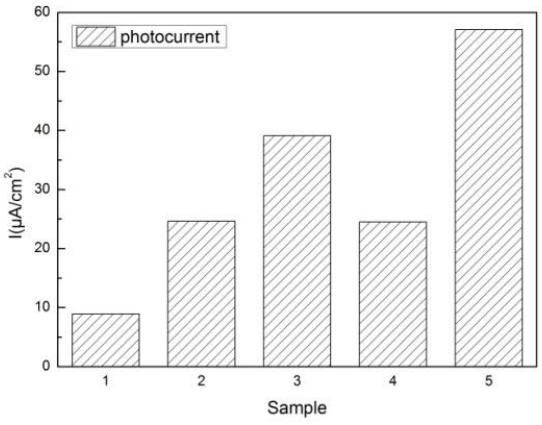

Figure 37. Photocurrents from CA measurements in Fig. 36

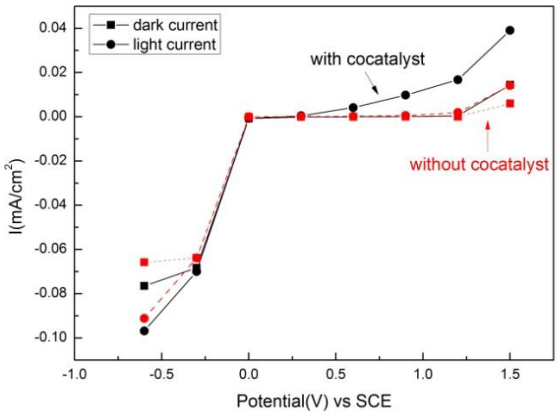

Figure 38. Photocurrents obtained from CA performed at different voltage bias on CHP with and without RuO_2

To further probe the photoelectrochemical properties of CHP, hole scavengers were added to the electrolyte. Methanol and hydrogen peroxide are often used as hole scavengers since their standard redox potentials are less positive than that for water oxidation (E^0 = +0.02 V vs. NHE for CO_2/CH_3OH and E^0 = +0.68 V vs. NHE for O_2/H_2O_2). Thus two CA measurements for CHP film on FTO were performed by adding 10 vol% methanol or 0.75 vol % hydrogen peroxide to the electrolyte and applying a 1.5 V vs. SCE bias (Figure 36 (4) and (5)). In many cases, materials limited by slow water oxidation kinetics (such as $BiVO_4$ [76] and Fe_2O_3 [77]) show higher photocurrents and lower photocurrent onset potential when illuminated in the presence of a hole scavenger, indicating that charge separation is not an issue. These measurements can thus help identify the limiting process in the photoelectrochemical activity of a material. The photocurrent was increased to 24.5 μA/cm^2 and 57.1 μA/cm^2, respectively, due to the additional hole scavengers. Using H_2O_2 as a hole scavenger resulted in the

highest photocurrent out of all the conditions tested, indicating that CHP may be particularly active for this reaction. The activation of H_2O_2 for hydroxylation of phenol over CHP[41] was suggested to be mediated by the intrinsic OH group in CHP, which allowed for a five-membered ring intermediate to form between Cu^{2+}-OH and H_2O_2. In the case of H_2O_2 oxidation, a similar intermediate may form except with O_2 as the product.

To better characterize the potential of CHP as a catalyst for the oxygen evolution reaction (OER), linear scanning voltammetry (LSV) measurements were performed on CHP films in Na_3PO_4 electrolytes, which was chosen since this was the electrolyte used in photocatalytic water oxidation studies performed on another phosphate containing material, Ag_3PO_4 [39]. Figure 39 compares the LSV data of three CHP films coated on FTO compared to bare FTO under chopped light in 0.02 M Na_3PO_4 (pH 5) electrolyte. From cross-section SEM, the films were determined to have a thickness of about 80 μm (for CHP-1), 10-40 μm (for CHP-2), and 0.5-3 μm (for CHP-3). A small photocurrent was observed for the thinner CHP films, on the order of 1 $\mu A/cm^2$, and this was lower than the photocurrent observed for bare FTO. The larger dark current on the CHP sample greater than ~1.3 V vs. Ag/AgCl compared to the bare FTO suggests that CHP can also function as an electrocatalyst for OER. At pH 5, the thermodynamic potential for water oxidation is at 1.23 V vs. RHE, indicating that the CHP has ~560 mV overpotential as an OER catalyst. However, the results indicate that the film preparation and thickness play a large role in the current onset potential as well as the current density. This is reasonable considering that CHP has strong

ionic bonding and may have poor electronic conductivity, leading to transport issues in thick films.

XRD of the CHP after LSV measurements in the pH 5 electrolyte did not show any change, indicating the CHP is stable (Fig. 40). When the pH of the electrolyte was increased to 12 with NaOH, the current onset potential decreased to 0.8 V vs. Ag/AgCl (1.71 V vs. RHE) (Fig. 41), which matches the shift expected for a Nernstian response of 59 mV per pH change. And XRD of the CHP after measurements in the pH electrolyte also did not show any change , indicating the CHP is stable in alkaline pH 12 (Fig. 42). However, performing LSV in pH 13 solutions resulted in a color change in the CHP films from light green to black. To better understand this, XRD was performed on CHP powder that was treated with KOH solutions (pH 13). After treatment for 1 hour, some $Cu(OH)_2$ peaks were observed along with those for CHP; for longer times, the CHP transformed to CuO and Cu_2O (Fig. 43).

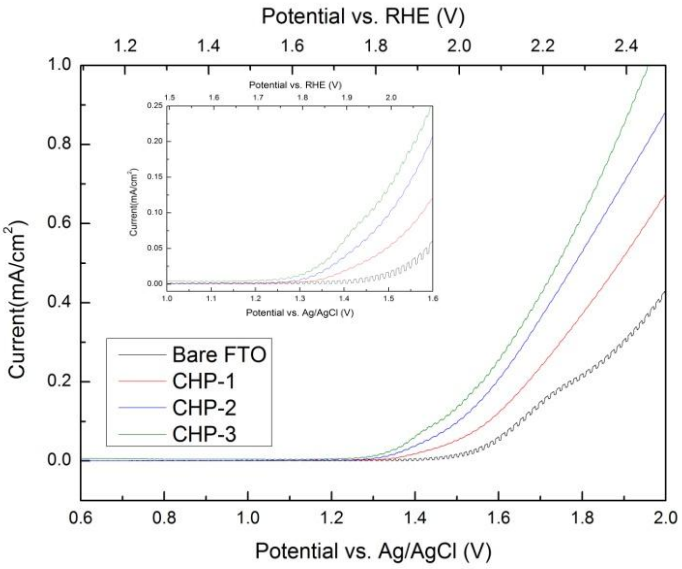

Figure 39. LSV of CHP films on FTO in 0.02 M Na_3PO_4 (pH 5) under chopped light, with inset showing zoomed in region

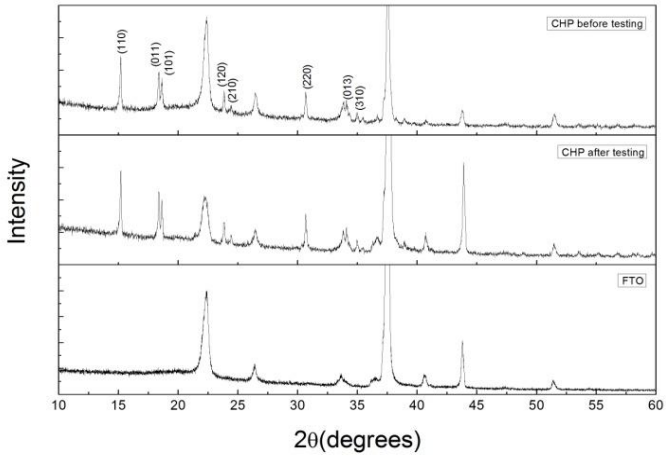

Figure 40. XRD of CHP before and after testing in pH 5 Na_3PO_4

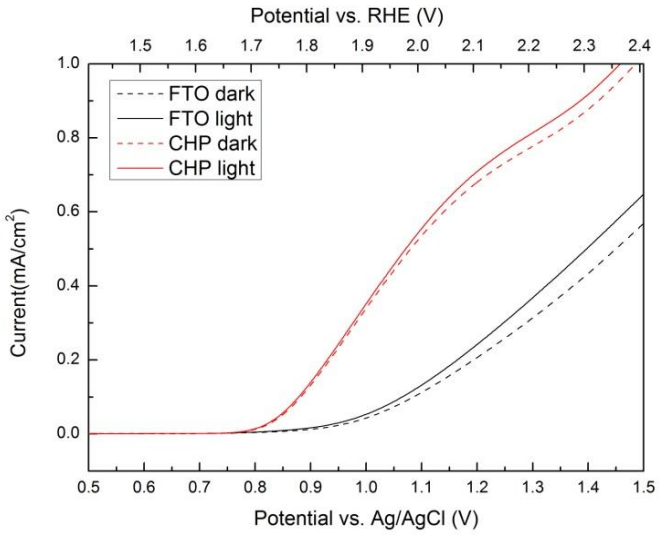

Figure 41. LSV of CHP in pH 12 electrolyte under light and dark conditions compared to bare FTO

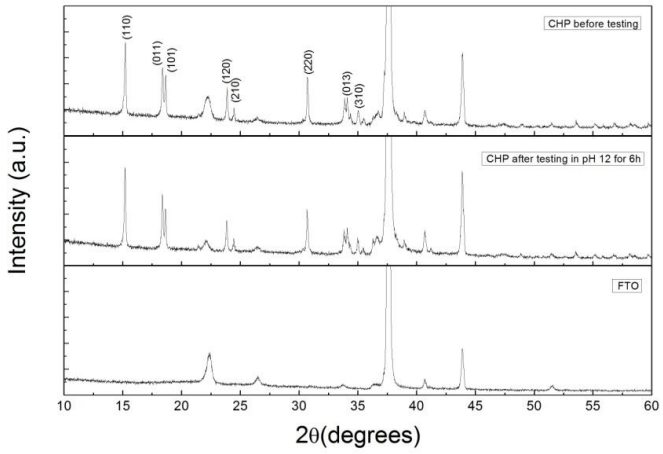

Figure 42. XRD of CHP before and after testing in pH 12 Na_3PO_4

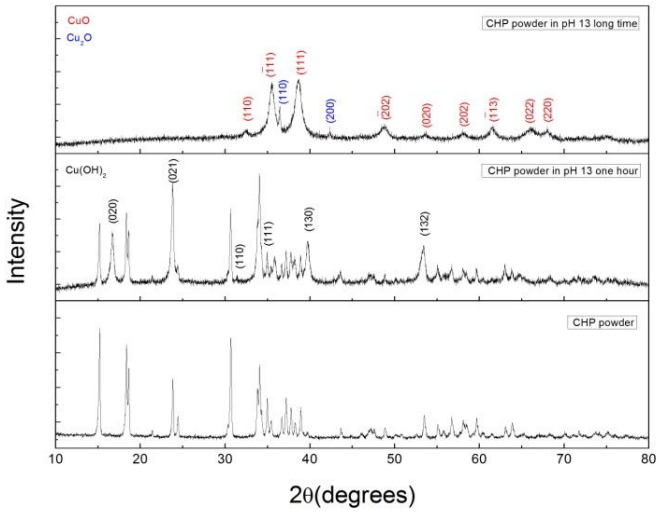

Figure 43. XRD of CHP after testing in pH 13 KOH

3.6. Photocatalytic Oxygen Evolution

To confirm the O_2 production, which is often suppressed in acidic or neutral electrolytes by anion oxidation[57,78], water oxidation under UV-light was performed in CHP suspension (1 g/L). Figure 44 compares oxygen generated under light condition with CHP as a catalyst as well as without CHP in light condition and with CHP in dark condition as a control. No oxygen increase was observed for the experiment without illumination. A small increase in O_2 of ~1μmol/L was observed when the electrolyte was illuminated without CHP , probably because the long illumination time led to an increase in electrolyte temperature, which decreased the solubility of oxygen in water. Approximately 2 μmol/L increase in oxygen concentration was observed for the electrolyte containing CHP under light irradiation. The difference between the one with CHP

and the one without CHP is quite small and the result is greatly influenced by the increase in temperature from the heat of the light irradiation.

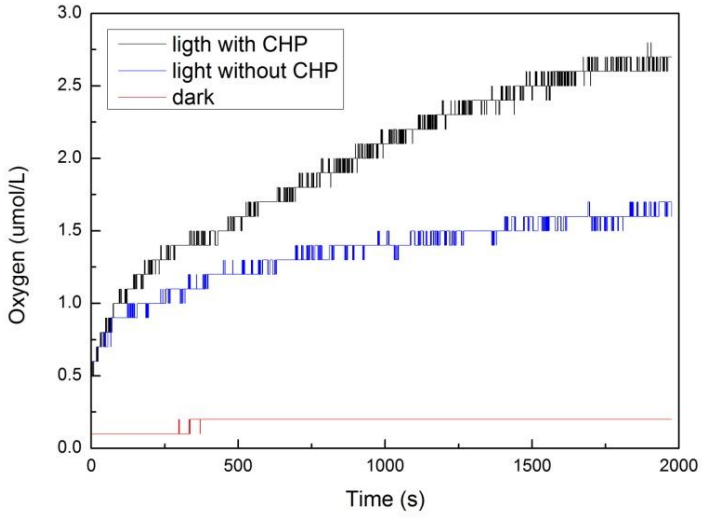

Figure 44. Photocatalytic oxygen production under light condition with CHP (black curve) and without CHP (blue curve) and a control with CHP in dark condition(red curve)

3.7. Electrocatalytic Water Oxidation

To better evaluate the oxygen evolution reaction (OER) activity of CHP and confirm the O_2 production as well as to eliminate the influence of illumination, electrocatalytic water oxidation was performed on the thinnest CHP coating on FTO (CHP-3). Although the CHP powder displayed photocurrent in the $FeCl_3$, MV^{2+}, and chopped light LSV measurements, the small magnitude made O_2 detection difficult as mentioned above. Furthermore, the large bandgap of CHP precluded the use of $AgNO_3$ as a sacrificial electron scavenger for

photocatalytic O_2 production from suspensions of CHP powder, due to the UV-light activated reduction of Ag^+ to Ag^0. This is illustrated in the SEM image in Figure 45(a), which shows the CHP after long illumination times when it was suspended with $AgNO_3$ as a sacrificial electron scavenger. The SEM shows small spherical particles accumulated on the rod-like CHP particles, which indicated that Ag^0 was formed the reduction of $AgNO_3$ under UV-light. This was confirmed with EDS (Fig. 45(b)), which shows a high concentration of Ag on the small particles area. $FeCl_3$ was also not a suitable electron scavenger due to its instability (i.e. precipitation) at long irradiation times unless in acidic pH solutions[76] in which CHP was not found to be stable. Therefore, CHP films were evaluated for OER in dark conditions in a pH 12 solution of 0.02 M Na_3PO_4 under a 1 V vs. Ag/AgCl applied bias. Based on the LSV results, the CHP electrode displayed a ~0.35 mA/cm^2 current at this potential, while bare FTO displayed only ~0.05 mA/cm^2 (Fig. 41). The results are shown in Figure 46, in which ~33 µmol O_2 /mg CHP was produced after 2900 sec. The chronoamperometry results (Fig. 47) showed a current of ~0.42 mA/cm^2, indicating a Faradaic efficiency of ~76% for water oxidation. The turnover frequency (TOF) of 1.68 molecules O_2 /s•nm (equivalent to 2.79 µmol O_2/s•m^2 and 2.74 x 10^{-3} mol O_2/s•mol CHP) was determined based on the projected surface area of the CHP particles and the amount of CHP used.

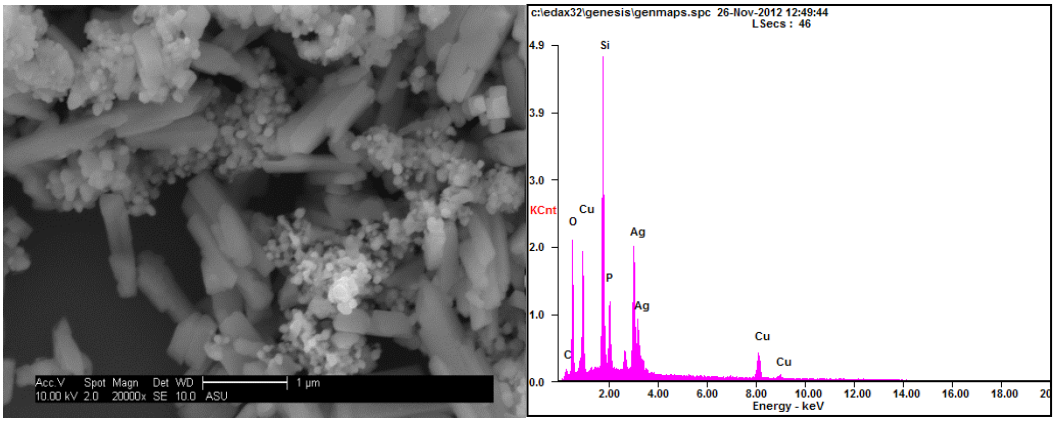

(a) (b)

Figure 45. SEM image of CHP with $AgNO_3$ added in the suspension after the long time illumination (a) and (b) EDS indicated that small spherical particles were Ag^0

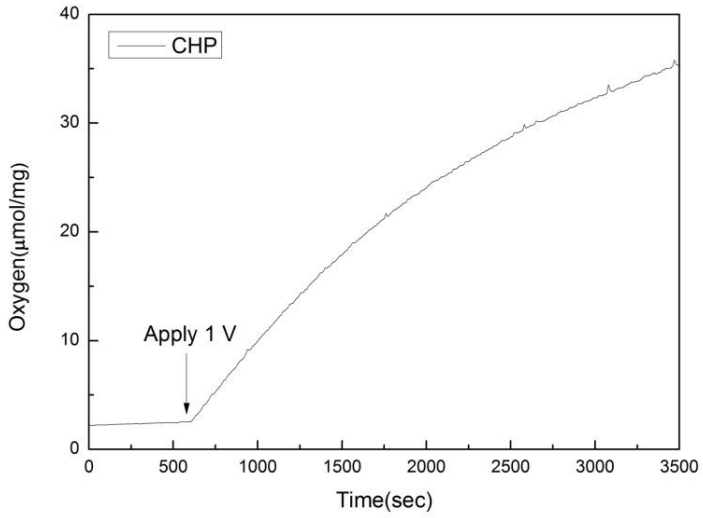

Figure 46. Electrochemical oxygen production on CHP-3 under a 1 V vs. Ag/AgCl bias

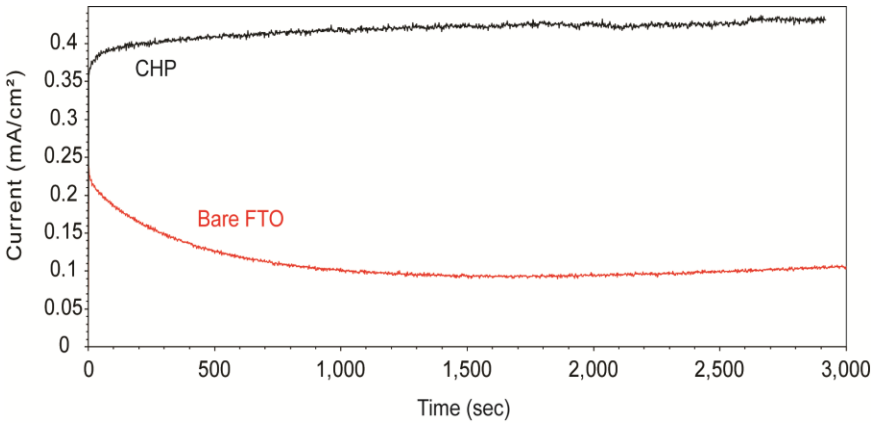

Figure 47. Chronoamperometry measurement of CHP and bare FTO at a bias voltage of 1 V vs. Ag/AgCl in pH 12 Na_3PO_4

To be more specific, the theoretical amount of O_2 expected was determined using Faraday's law and an electrode area of 6.912 cm^2, total electrolysis time of 2900 sec, and observed current density of 0.42 mA/cm^2. The theoretical amount oxygen was calculated.

The signal measured from the fluorescence sensor (% O_2) was converted to dissolved O_2 (µmol/L) using the equations offered by the Neofox (the O_2 sensor) manual, as shown below:

$$[PPM] = e^{A1+A2\bullet T1+A3\bullet \ln(T2)+A4\bullet T2+SC\bullet(B1+B2\bullet T2+B3\bullet T2\bullet T2)} \bullet C\bullet PO2/D$$

$$[\mu mol/L] = 1000 / 31\bullet[PPM]$$

A1,A2,A3,A4,B1,B2,B3,C,D are constants, hardcoded in the firmware:

A1 = 173.9894

A2 = 255.5907

A3 = 146.4813

A4 = -22.204

B1 = -0.037362

B2 = 0.016504

B3 = -0.0020564

C = 0.032

D = 20.9

T1 is 100 divided by the temperature (in Kelvin)

T2 is the temperature (in Kelvin) divided by 100 (Temperature here is determined as 298 K)

SC is the "salinity correction factor", which is estimated as 1 in alkali solution

PO2 is the "percent oxygen", which is directly obtained from the fluorescence sensor

The real number of moles of O_2 produced was determined given the volume of electrolyte used (0.15 L). The ratio of the observed to theoretical amount of O_2 gave a Faradaic efficiency of 76.31 %. Using this Faradaic efficiency and 4 electrons required for water oxidation, the number of O_2 molecules produced per second was determined to be 3.46×10^{15}. Using the measured BET surface area of 4.11 m^2/g and the mass of CHP loaded onto the FTO substrate (about 0.5 mg, based on the concentration of the CHP paste used and the volume loaded), the total projected surface area of the CHP was calculated as 2.058×10^{15} nm^2. The turnover frequency is thus determined to be 1.68 molecules O_2 s^{-1} nm^{-2}.

Although it is difficult to compare TOF of various catalyst materials due to differences in experimental measurement conditions, these TOF numbers fall in

the range of other water oxidation catalysts currently under investigation by many groups (e.g. 10^{-2} to 10^{-6} mol O_2/s•mol for cobalt and manganese oxide based materials)[79]. Since about 8 mol O_2 was produced for each mol of CHP, this suggests that the O_2 was produced from electrochemical water oxidation and not from CHP decomposition. This was confirmed by performing XRD on CHP films after the CA was performed for 6 h. As shown in Fig. 42, no new peaks indicative of CHP decomposition products were observed.

4. Conclusions

Different morphologies of the copper hydroxyphosphate material libethenite (CHP) were synthesized successfully using hydrothermal synthesis and precipitation method. It can be conclude that for hydrothermal synthesis, $CuSO_4$ is a better reactant than CuCl used for synthesizing pure CHP, which can be obtained at 200 ℃ for 2 h. This is because CuCl is easy to become Cu_2O once dissolved in water, but it is hard to convert Cu_2O to CHP. The particle size cannot be adjusted by lowering the reaction temperature since the amorphous blue phase which formed first cannot convert to CHP completely at lower temperatures. By comparing the hydrothermal synthesis and precipitation method using $CuSO_4$ as reactant, it is clear to see that precipitation method is better to synthesize CHP at lower temperature and the CHP particles are more uniform probably because of stirring while reaction.

The properties of CHP were investigated using a series of electrochemical and photoelectrochemical analysis. A conduction band edge slightly positive of the H^+/H_2 reduction potential was observed, and Mott-Schottky analysis indicated that CHP showed n-type behavior. A film thickness dependence on the CHP photocurrent and electrocatalytic performance for O_2 production suggests that the performance of CHP is hampered by its poor electronic conductivity due to its ionic bonding characteristics. Water oxidation using an external voltage bias and light-activation confirmed that CHP does display activity for electrochemical O_2 production. These results indicate that materials with Jahn-Teller distortions may be attractive for the development of higher activity water oxidation catalysts.

As crystal structure, electronic structure, defect and surface considerations can play a large role in the activity of a photocatalyst, the underlying reason for the low photocurrents in CHP is still unknown, despite the high activity observed for photocatalytic dye degradation. Future work will explore the contributions of each of these factors to the electrochemical and photoelectrochemical characteristics of this material. Studies on how size and shape dependence affect the electrocatalytic activity may also be worthwhile.

REFERENCES

1. Cho, I. S., D. W. Kim, S. Lee, C. H. Kwak, S. Bae, J. H. Noh, S. H. Yoon, H. S. Jung, D. Kim, and K. Hong. "Synthesis of Cu_2PO_4OH Hierarchical Superstructures with Photocatalytic Activity in Visible Light." *Adv. Funct. Mater.* 18, no. 15 (2008): 2154.

2. Kwak, C. H., I. S. Cho, S. Lee, J. S. An, and K. S. Hong. "Hydrothermal Synthesis, Characterization and Photocatalytic Properties of Cu_2PO_4OH with Hierarchical Morphologies." *Journal of Nanoscience and Nanotechnology* 10, (2010): 1185-1190.

3. "Solar Energy Perspectives: Executive Summary." International Energy Agency, http://www.iea.org/Textbase/npsum/solar2011SUM.pdf.

4. *Solar Fuels and Artificial Photosynthesis: Science and Innovation to Change our Future Energy Options*: Advancing the Chemical Sciences, 2012.

5. Butler, M. A. and D. S. Ginley. "Principles of Photoelectrochemical, Solar Energy Conversion." *Journal of Materials Science* 15, no. 1 (1980): 1-19.

6. Nozik, Arthur J. "Photoelectrochemistry: Applications to Solar Energy Conversion." *Annual Review of Physical Chemistry* 29, no. 1 (1978): 189-222.

7. Schiavello, M. "Semiconductor Electrodes and their Interaction with Light." In *Photoelectrochemistry, Photocatalysis and Photoreactors Fundamentals and Developments*, edited by Mario Schiavello, 39. The Netherlands: Dordrecht, 1985.

8. Becquere, E. "Mémoire Sur Les Effets Électriques Produits Sous l'Influence Des Rayons Solaires." *Compt. Rend. Acad. Sci.* 9, (1839): 561.

9. Brattain, W. H. and C. G. B. Garrett. *Bell System Tech. J.* 34, (1955): 129.

10. Fujishima, A., K. Honda, and S. S. Kikuchi. " Photosensitized Electrolytic Oxidation on Semiconducting n-Type TiO_2 electrode ." *Kogyo Kagaku Zasshi* 72, (1969): 108.

11. De Haart, L., A. J. De Vries, and G. Blasse. "On the Photoluminescence of Semiconducting Titanates Applied in Photoelectrochemical Cells." *Journal of Solid State Chemistry* 59, (1985): 261.

12. Hoffmann, M. R., S. T. Martin, W. Choi, and D. W. Bahnemann. "Environmental Applications of Semiconductor Photocatalysis." *Chemical Reviews* 95, no. 1 (1995): 69-96.

13. Linsebigler, A. L., G. Lu, and J. T. Yates. "Photocatalysis on TiO_2 Surfaces: Principles, Mechanisms, and Selected Results." *Chemical Reviews* 95, no. 3 (1995): 735-758.

14. Mills, A. and L. H. Stephen. "An Overview of Semiconductor Photocatalysis." *Journal of Photochemistry and Photobiology.A, Chemistry* 108, no. 1 (1997): 1-35.

15. Carp, O., C. L. Huisman, and A. Reller. "Photoinduced Reactivity of Titanium Dioxide." *Progress in Solid State Chemistry* 32, no. 1 (2004): 33-177.

16. Herrmann, J. M. "Heterogeneous Photocatalysis: Fundamentals and Applications to the Removal of various Types of Aqueous Pollutants." *Catalysis Today* 53, no. 1 (1999): 115-129.

17. Cao, F., G. Oskam, G. J. Meyer, and P. C. Searson. "Electron Transport in Porous Nanocrystalline TiO_2 Photoelectrochemical Cells." *The Journal of Physical Chemistry* 100, no. 42 (1996): 17021-17027.

18. Asahi, R., T. Morikawa, T. Ohwaki, K. Aoki, and Y. Taga. "Visible-Light Photocatalysis in Nitrogen-Doped Titanium Oxides." *Science* 293, no. 5528 (2001): 269-271.

19. In, S., A. Orlov, R. Berg, F. Garcia, S. Pedrosa-Jimenez, M. S. Tikhov, D. S. Wright, and R. M. Lambert. "Effective Visible Light-Activated B-Doped and B, N-Codoped TiO_2 Photocatalysts." *Journal of the American Chemical Society* 129, no. 45 (2007): 13790-13791.

20. Hu, C. C. and H. S. Teng. "Structural Features of p-Type Semiconducting NiO as a Co-Catalyst for Photocatalytic Water Splitting." *Journal of Catalysis* 272, no. 1 (2010): 1-8.

21. Li, Q. Y., T. Kako, and J. H. Ye. "WO_3 Modified Titanate Network Film: Highly Efficient Photo-Mineralization of 2-Propanol Under Visible Light Irradiation." *Chemical Communications* 46, no. 29 (2010): 5352-5354.

22. Jang, J. S., S. H. Choi, H. Park, W. Choi, and J. S. Lee. "A Composite Photocatalyst of CdS Nanoparticles Deposited on TiO_2 Nanosheets."

Journal of Nanoscience and Nanotechnology 6, no. 11 (2006): 3642-3646.

23. Reiche, H., W. W. Dunn, and A. J. Bard. "Heterogeneous Photocatalytic and Photosynthetic Deposition of Copper on Titanium Dioxide and Tungsten (VI) Oxide Powders." *Journal of Physical Chemistry* 83, no. 17 (1979): 2248-2251.

24. Cesar, I., K. Sivula, A. Kay, R. Zboril, and M. Grätzel. "Influence of Feature Size, Film Thickness, and Silicon Doping on the Performance of Nanostructured Hematite Photoanodes for Solar Water Splitting." *The Journal of Physical Chemistry C* 113, no. 2 (2008): 772-782.

25. Tahir, A. A., K. G. U. Wijayantha, S. Saremi-Yarahmadi, M. Mazhar, and V. Mckee. "Nanostructured α-Fe_2O_3 Thin Films for Photoelectrochemical Hydrogen Generation." *Chem. Mater.* 21, (2009): 3763.

26. Prakasam, H. E., O. K. Varghese, M. Paulose, G. K. Mor, and C. A. Grimes. "Synthesis and Photoelectrochemical Properties of Nanoporous Iron (III) Oxide by Potentiostatic Anodization." *Nanotechnology* 17, no. 17 (2006): 4285.

27. Mohapatra, S. K., S. E. John, S. Banerjee, and M. Misra. "Water Photooxidation by Smooth and Ultrathin α-Fe_2O_3 Nanotube Arrays." *Chemistry of Materials* 21, no. 14 (2009): 3048-3055.

28. LaTempa, T. J., X. Feng, M. Paulose, and C. A. Grimes. "Temperature-Dependent Growth of Self-Assembled Hematite (α-Fe_2O_3) Nanotube Arrays: Rapid Electrochemical Synthesis and Photoelectrochemical Properties." *The Journal of Physical Chemistry C* 113, no. 36 (2009): 16293-16298.

29. Beermann, N., L. Vayssieres, S. - E Lindquist, and A. Hagfeldt. "Photoelectrochemical Studies of Oriented Nanorod Thin Films of Hematite." *Journal of the Electrochemical Society* 147, no. 7 (2000): 2456-2461.

30. Kay, A., I. Cesar, and M. Grätzel. "New Benchmark for Water Photooxidation by Nanostructured α-Fe_2O_3 Films." *Journal of the American Chemical Society* 128, no. 49 (2006): 15714-15721.

31. Kleiman-Shwarsctein, A., Y. S. Hu, G. D. Stucky, and E. W. McFarland. "NiFe-Oxide Electrocatalysts for the Oxygen Evolution Reaction on Ti

Doped Hematite Photoelectrodes." *Electrochemistry Communications* 11, no. 6 (2009): 1150-1153.

32. Walter, M. G., E. L. Warren, J. R. McKone, S. W. Boettcher, Q. Mi, E. A. Santori, and N. S. Lewis. "Solar Water Splitting Cells." *Chemical Reviews* 110, no. 11 (2010): 6446-6473.

33. Chen, Z. B., T. F. Jaramillo, T. G. Deutsch, A. Kleiman-Shwarsctein, A. J. Forman, N. Gaillard, R. Garland, K. Takanabe, C. Heske, and M. Sunkara. "Accelerating Materials Development for Photoelectrochemical Hydrogen Production: Standards for Methods, Definitions, and Reporting Protocols." *J.Mater.Res* 25, no. 1 (2010): 3.

34. Turner, J., G. Sverdrup, M. K. Mann, P. ‐C Maness, B. Kroposki, M. Ghirardi, R. J. Evans, and D. Blake. "Renewable Hydrogen Production." *International Journal of Energy Research* 32, no. 5 (2008): 379-407.

35. Huminicki, D. M. C. and F. C. Hawthorne. "The Crystal Chemistry of the Phosphate Minerals." *Reviews in Mineralogy and Geochemistry* 48, no. 1 (2002): 123-253.

36. Kanan, M. W. and D. G. Nocera. "In Situ Formation of an Oxygen-Evolving Catalyst in Neutral Water Containing Phosphate and Co^{2+} ." *Science* 321, no. 5892 (2008): 1072-1075.

37. Surendranath, Y., M. W. Kanan, and D. G. Nocera. "Mechanistic Studies of the Oxygen Evolution Reaction by a Cobalt-Phosphate Catalyst at Neutral pH." *Journal of the American Chemical Society* 132, no. 46 (2010): 16501-16509.

38. Zhong, D. K. and D. R. Gamelin. "Photoelectrochemical Water Oxidation by Cobalt Catalyst ("Co− Pi")/α-Fe_2O_3 Composite Photoanodes: Oxygen Evolution and Resolution of a Kinetic Bottleneck." *Journal of the American Chemical Society* 132, no. 12 (2010): 4202-4207.

39. Yi, Z. G., J. H. Ye, N. Kikugawa, T. Kako, S. Ouyang, H. Stuart-Williams, H. Yang, et al. "An Orthophosphate Semiconductor with Photooxidation Properties Under Visible-Light Irradiation." *Nature Materials* 9, (2010): 559-564.

40. Meng, X., K. Lin, J. Sun, M. Yang, D. Jiang, and F. S. Xiao. "Catalytic Epoxidation of Styrene Over Copper Hydroxyphosphate Cu_2 (OH) PO_4." *Catalysis Letters* 71, no. 3/4 (2001): 241-244.

41. Xiao, F. S., J. Sun, X. Meng, R. Yu, H. Yuan, J. Xu, T. Song, D. Jiang, and R. Xu. "Synthesis and Structure of Copper Hydroxyphosphate and its High Catalytic Activity in Hydroxylation of Phenol by H_2O_2." *Journal of Catalysis* 199, no. 2 (2001): 273.

42. Meng, X., K. Lin, X. Yang, Z. Sun, D. Jiang, and F. S. Xiao. "Catalytic Oxidation of Olefins and Alcohols by Molecular Oxygen Under Air Pressure Over Cu_2 (OH) PO_4 and Cu_4O (PO4) $_2$ Catalysts." *Journal of Catalysis* 218, no. 2 (2003): 460.

43. Xu, Y., C. Wang, and S. Yang. "Uniform Copper Hydroxyphosphate Microstructures with Tunable Size: Synthesis by a Facile Surfactant-Free Hydrothermal Route and Photocatalytic Properties." *Materials Letters* (2012).

44. Wang, G., B. Huang, X. Ma, Z. Wang, X. Qin, X. Zhang, Y. Dai, and M. H. Whangbo. "$Cu_2(OH)PO_4$, a Near‐Infrared‐Activated Photocatalyst." *Angewandte Chemie* 125, no. 18 (2013): 4910-4913.

45. Dewald, J. F. "The Charge Distribution at the Zinc Oxide-Electrolyte Interface." *The Journal of Physics and Chemistry of Solids* 14, (-07, 1960): 155-161.

46. Gopalakrishna, G. S., M. J. Mahesh, K. G. Ashamanjari, and P. J. Shashidhara. "Structure, Thermal and Magnetic Characterization of Hydrothermal Synthesized $Li_2CuP_2O_7$ Crystals." *Materials Research Bulletin* 43, no. 5 (2008): 1171-1178.

47. Ji, F., C. L. Li, and J. H. Zhang. "Hydrothermal Synthesis of Li_9Fe_3 $(P_2O_7)_3(PO_4)_2$ Nanoparticles and their Photocatalytic Properties Under Visible-Light Illumination." *ACS Applied Materials & Interfaces* 2, no. 6 (2010): 1674-1678.

48. Hiroshi, H., K. Maeda, R. Abe, A. Ishikawa, J. Kubota, and K. Domen. "Photoresponse of GaN:ZnO Electrode on FTO Under Visible Light Irradiation." *Bulletin of the Chemical Society of Japan* 82, no. 3 (2009): 401-407.

49. Abe, Ryu, M. Higashi, and K. Domen. "Facile Fabrication of an Efficient Oxynitride TaON Photoanode for overall Water Splitting into H and O Under Visible Light Irradiation." *Journal of the American Chemical Society* 132, no. 34 (-09, 2010): 11828-11829.

50. Escudero, J. C., S. Cervera-March, J. Giménez, and R. Simarro. "Preparation and Characterization of $Pt(RuO_2)/TiO_2$ Catalysts: Test in a Continuous Water Photolysis System." *Journal of Catalysis* 123, no. 2 (-06, 1990): 319-332.

51. Ito, S., P. Chen, P. Comte, M. K. Nazeeruddin, P. Liska, P. Pechy, and M. Grätzel. "Fabrication of Screen - printing Pastes from TiO_2 Powders for Dye - sensitised Solar Cells." *Progress in Photovoltaics: Research and Applications* 15, no. 7 (2007): 603-612.

52. Park, H. "Photoelectrochemical Investigation on Electron Transfer Mediating Behaviors of Polyoxometalate in UV-Illuminated Suspensions of TiO_2 and Pt/TiO_2." *The Journal of Physical Chemistry.B* 107, no. 16 (-04, 2003): 3885-3890.

53. Ward, M. D., J. R. White, and A. J. Bard. "Electrochemical Investigation of the Energetics of Particulate Titanium Dioxide Photocatalysts. the Methyl Viologen-Acetate System." *Journal of the American Chemical Society* 105, no. 1 (1983): 27-31.

54. White, J. R. and A. J. Bard. "Electrochemical Investigation of Photocatalysis at Cadmium Sulfide Suspensions in the Presence of Methylviologen." *The Journal of Physical Chemistry* 89, no. 10 (1985): 1947-1954.

55. Cardon, F. and W. P. Gomes. "On the Determination of the Flat-Band Potential of a Semiconductor in Contact with a Metal Or an Electrolyte from the Mott-Schottky Plot." *Journal of Physics.D, Applied Physics* 11, no. 4 (1978): L63; 003-L67.

56. Surendranath, Y., M. Dincă, and D. G. Nocera. "Electrolyte-Dependent Electrosynthesis and Activity of Cobalt-Based Water Oxidation Catalysts." *J.Am.Chem.Soc* 131, no. 7 (2009): 2615-2620.

57. Mi, Q. X., A. Zhanaidarova, B. S. Brunschwig, H. B. Gray, and N. S. Lewis. "A Quantitative Assessment of the Competition between Water and Anion Oxidation at WO_3 Photoanodes in Acidic Aqueous

Electrolytes." *Energy & Environmental Science* 5, no. 2 (2012): 5694-5700.

58. Kresse, G. and D. Joubert. "From Ultrasoft Pseudopotentials to the Projector Augmented-Wave Method." *Physical Review B* 59, no. 3 (1999): 1758.

59. Zema, M., S. C. Tarantino, and A. M. Callegari. "Thermal Behaviour of Libethenite from Room Temperature Up to Dehydration." *Mineralogical Magazine* 74, no. 3 (2010): 553-565.

60. Xu, J. and D. F. Xue. "Fabrication of Copper Hydroxyphosphate with Complex Architectures." *The Journal of Physical Chemistry B* 110, no. 15 (2006): 7750-7756.

61. Dutoit, E. C., R. L. Van Meirhaeghe, F. Cardon, and W. P. Gomes. "Investigation on the Frequency - dependence of the Impedance of the nearly Ideally Polarizable Semiconductor Electrodes CdSe, CdS and TiO_2." *Berichte Der Bunsengesellschaft Für Physikalische Chemie* 79, no. 12 (1975): 1206-1213.

62. Minami, T. "New N-Type Transparent Conducting Oxides." *MRS Bulletin* 25, no. 8 (2000): 38-44.

63. Kim, Y. I., S. J. Atherton, E. S. Brigham, and T. E. Mallouk. "Sensitized Layered Metal Oxide Semiconductor Particles for Photochemical Hydrogen Evolution from Nonsacrificial Electron Donors." *Journal of Physical Chemistry (1952)* 97, no. 45 (-11, 1993): 11802-11810.

64. Kubelka, P. "New Contributions to the Optics of Intensely Light-Scattering Materials Part I." *Journal of the Optical Society of America (1930)* 38, no. 5 (-05, 1948): 448.

65. Christy, A. A., O. M. Kvalheim, and R. A. Velapodi. "Quantitative Analysis in Diffuse Reflectance Spectrometry: A Modified Kubelka-Munk Equation." *Vibrational Spectroscopy* 9, no. 1 (-05, 1995): 19-27.

66. Elliott, R. J. "Intensity of Optical Absorption by Excitons." *Physical Review* 108, no. 6 (-12, 1957): 1384-1389.

67. Tauc, J., R. Grigorov, and A. Vancu. "Optical Properties and Electronic Structure of Amorphous Germanium." *Physica Status Solidi.B, Basic Research* 15, no. 2 (1966): 627-637.

68. Tauc, J., A. Menth, and D. L. Wood. "Optical and Magnetic Investigations of the Localized States in Semiconducting Glasses." *Physical Review Letters* 25, no. 11 (-09, 1970): 749-752.

69. Park, Y., N. J. Singh, K. S. Kim, T. Tachikawa, T. Majima, and W. Choi. "Fullerol-Titania Charge-Transfer-Mediated Photocatalysis Working Under Visible Light." *Chemistry : A European Journal* 15, no. 41 (-10, 2009): 10843-10850.

70. Kraeutler, B. and A. J. Bard. "Heterogeneous Photocatalytic Decomposition of Saturated Carboxylic Acids on Titanium Dioxide Powder. Decarboxylative Route to Alkanes." *Journal of the American Chemical Society* 100, no. 19 (-09, 1978): 5985-5992.

71. Byrne, J. A., B. R. Eggins, S. M. Dunlop, and S. Linquette-Mailley. "The Effect of Hole Acceptors on the Photocurrent Response of Particulate TiO_2 Anodes." *Analyst (London)* 123, no. 10 (1998): 2007-2012.

72. Park, H. and W. Choi. "Effects of TiO_2 Surface Fluorination on Photocatalytic Reactions and Photoelectrochemical Behaviors." *The Journal of Physical Chemistry B* 108, no. 13 (2004): 4086-4093.

73. Matsumoto, Y., M. Omae, I. Watanabe, and E. Sato. "Photoelectrochemical Properties of the Zn-Ti-Fe Spinel Oxides." *Journal of the Electrochemical Society* 133, no. 4 (1986): 711.

74. Matsumoto, Y. "Energy Positions of Oxide Semiconductors and Photocatalysis with Iron Complex Oxides." *Journal of Solid State Chemistry* 126, no. 2 (-11, 1996): 227-234.

75. Yeo, R. S., J. Orehotsky, W. Visscher, and S. Srinivasan. "Ruthenium-Based Mixed Oxides as Electrocatalysts for Oxygen Evolution in Acid Electrolytes." *Journal of the Electrochemical Society* 128, no. 9 (1981): 1900.

76. Abdi, F. and R. van de Krol. "Nature and Light Dependence of Bulk Recombination in Co-Pi-Catalyzed BiVO Photoanodes." *Journal of Physical Chemistry.C* 116, no. 17 (-05, 2012): 9398-9404.

77. Dotan, H., K. Sivula, M. Gratzel, A. Rothschild, and S. C. Warren. "Probing the Photoelectrochemical Properties of Hematite (α-Fe_2O_3) Electrodes using Hydrogen Peroxide as a Hole Scavenger." *Energy & Environmental Science* 4, no. 3 (2011): 958.

78. Hill, J. C. and K. S. Choi. "Effect of Electrolytes on the Selectivity and Stability of N-Type WO_3 Photoelectrodes for use in Solar Water Oxidation." *The Journal of Physical Chemistry C* 116, no. 14 (2012): 7612-7620.

79. Robinson, D. M., Y. B. Go, M. Greenblatt, and G. C. Dismukes. "Water Oxidation by λ-MnO_2: Catalysis by the Cubical Mn_4O_4 Subcluster obtained by Delithiation of Spinel $LiMn_2O_4$." *Journal of the American Chemical Society* 132, no. 33 (2010): 11467-11469.